



On the completeness of interface descriptions and the consistency of blocked forces obtained in situ

J.W.R. Meggitt*, A.T. Moorhouse

Acoustics Research Centre, University of Salford, Greater Manchester M5 4WT, United Kingdom



ARTICLE INFO

Article history:

Received 19 August 2019
Received in revised form 24 March 2020
Accepted 25 March 2020

Keywords:

Blocked forces
Completeness
Consistency
Source characterisation
Excitation
Digital twins

ABSTRACT

Blocked forces can be used to describe, independently, the operational characteristics of a vibratory source. Their use within a computational model avoids the need to represent explicitly the complex mechanisms that lead to vibratory excitation. To obtain and apply an experimental blocked force with confidence it is important that likely sources of error are known, and measures of their severity are available. In this paper we introduce the notions of completeness and consistency, and detail their role in the introduction of systematic errors in a blocked force characterisation. Their mathematical origins are described and criteria to quantify their severity are proposed; the Interface Completeness Criterion (ICC), and the Measurement Consistency Criterion (MCC). These are illustrated through numerical and experimental examples. Completeness is related to the interface description adopted in a source characterisation (i.e. the number of degrees of freedom used). The ICC represents the quality of an interface description and can be quantified from in situ measurements, i.e. without having to remove the source from its assembly. Consistency is related to the underlying dynamics shared by active and passive quantities (whether measured or modelled). The issue of consistency is more general, completeness being a special case, and so a single criterion is hard to formulate. When an inconsistency arises between the blocked force of a vibration source and its corresponding free interface frequency response function matrix, the MCC provides a quantitative indication of its severity. Importantly, many of the concepts discussed apply equally in the context of experimental dynamic sub-structuring.

© 2020 The Author(s). Published by Elsevier Ltd. This is an open access article under the CC BY license (<http://creativecommons.org/licenses/by/4.0/>).

1. Introduction

This paper is concerned with the excitation of structural dynamic and vibro-acoustic models using experimentally determined blocked forces. In particular we investigate the conditions under which a reliable prediction may be obtained when using the blocked force as an equivalent excitation. In doing so we will introduce the notions of completeness and consistency, and discuss their role in the introduction systematic errors.

The present work is motivated by a general move towards virtual prototyping methodologies and the growing popularity of so-called 'Digital Twins' [1]. In the Digital Twin (DT) paradigm, a physical system (or 'Physical Twin') is accompanied by a digital counterpart, designed to exhibit phenomena observed in the Physical Twin (PT). The design and implementation of a DT is context dependent and will vary from one application to another. A notable example (and of principal interest here) is the predictive methodology component-based Transfer Path Analysis (TPA).

* Corresponding author.

Transfer Path Analysis is a general term used to describe a series of diagnostic and predictive methods applied in many industries to analyse the propagation of noise and vibration in complex built-up structures. Variants include classical- [2], in situ- [3], advanced- [4] and operational- [5], among others [6]. In a component-based TPA an assembly is sub-divided into a series of active and passive components, the dynamic properties of which are determined *separately* from one another. These are then combined as part of a computation model (or 'DT'), with the aim of predicting the assembled structure's operational response (this merger has previously been known as Virtual Acoustic Prototyping [7,8]). The resulting model may be complex, with multiple sub-components, each utilising disparate numerical, statistical or experimental descriptions [9]. Irrespective of its complexity, the model must provide an accurate estimate of the assembly's operational response if it is to be used as a predictive tool.

To achieve an accurate response prediction the assembled model must 1) correctly describe the assembly's passive properties (i.e. its response to a unit excitation) and 2) correctly model the excitation induced by its active components. Whilst numerical models are able to predict the passive properties of complex structures with reasonable accuracy, the mechanisms that lead to vibratory excitation often lay outside their capabilities. In a component-based TPA this issue is resolved by using an equivalent blocked force excitation, characterised experimentally, as an alternative to modelling the internal mechanisms of an active component.

Defined as the force required to constrain an active component's interface such that its velocity (also displacement and acceleration) is zero, the blocked force independently characterises the activity of a vibratory source [10]. Its independence allows for structural modifications to be made to an assembly without changing the source's operational characteristics, i.e. blocked forces are invariant to changes made in the receiver structure. In contrast, contact forces (as used in classical TPA) depend on the dynamics of the receiver structure and therefore cannot be used in the presence of a structural modification. Characterisation of the blocked force has been simplified in recent years by the development of an in situ procedure [11], which avoids the need for an infinitely rigid test bench. Posed as an inverse problem, the in situ blocked force approach [11] can be sensitive to numerical instabilities resulting from ill-conditioning, and the uncertainty arising from the experimental test procedure [12]. Beyond these issues, there exist two important notions that must be acknowledged if blocked forces are to be obtained and applied with confidence. These are; the *completeness* of the source-receiver interface description, and the *consistency* between the active (operational) and passive test phases. It is the aim of this paper to introduce these notions and highlight their importance in the characterisation and application of blocked forces.

Although we will consider completeness and consistency primarily from a blocked force perspective, it is important to note that many of the issues raised apply equally in the context of sub-structure coupling and decoupling. As an example, to successfully couple (or decouple) two sub-structures their separating interface must be characterised appropriately. This is clearly an interface completeness problem.

The remainder of this paper will be organised as follows. Section 2 will begin by reintroducing the blocked force and its in situ measurement procedure. In Section 3 the problem statement will be outlined and the notions of completeness and consistency described. Following this, Sections 4 and 5 will illustrate their mathematical origin, whilst providing criteria for their assessment and numerical examples of their application. Section 6 will go on to consider an experimental study, highlighting the aforementioned developments. Finally, Section 7 will draw some concluding remarks.

2. Blocked force as an independent source characterisation

The independent characterisation of vibratory sources (e.g. pumps, motors, etc.) has been of interest to those within the field of structural dynamics for many years [13]. Of the available quantities, there exist two fundamental (independent) descriptors of structural source activity. These are the blocked force and the free velocity [10]. The direct measurement of these quantities are, however, fraught with experimental difficulties and, until recently, neither had been considered a viable option for vibratory characterisation.¹

The blocked force is defined as the force required to restrain the coupling interface of a vibratory source such that its velocity (also displacement and acceleration) is zero,

$$\bar{\mathbf{f}}_{sc} = \mathbf{f}_{cc}|_{\mathbf{v}_{cc}=0} \quad (1)$$

where: lower-case subscript c represents the coupling interface degrees of freedom (DoFs) that separate source and receiver sub-structures (see Fig. 1); upper-case subscripts C and S represent the coupled assembly and the source sub-structure, respectively; and the over-bar accent is used to denote a *blocked* force, as opposed to a contact force. Noting the above, \mathbf{f}_{cc} may be read as the contact force present at the coupling interface of the coupled assembly, and $\bar{\mathbf{f}}_{sc}$ as the blocked force of the source sub-structure at the coupling interface. By blocking the interface DoFs c the dynamics of the receiver structure are unable to influence the blocked force. As such, it provides an *independent* description of structural source activity.

Note that blocked forces are typically defined at the separating interface between source and receiver sub-structures, i.e. remote from any internal vibration generating mechanisms. However, this interface is somewhat arbitrary, and chosen mostly for convenience. The blocked force may just as well be defined internally to the source sub-structure, perhaps over an enveloping surface that encloses the internal generating mechanisms [14].

¹ In this work we will consider the blocked force only. An account of the free velocity approach may be found in [1].

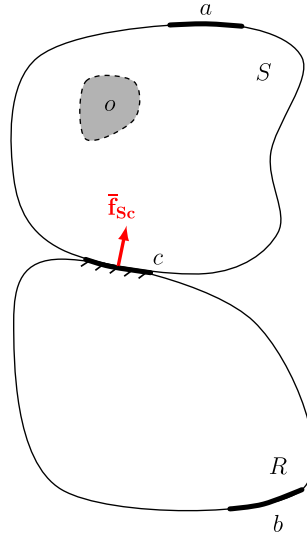


Fig. 1. Diagrammatic representation of source-receiver (SR) assembly and blocked force.

Assuming linearity and time invariance, the blocked force, defined at the interface DoFs c , can be related to the internal generating forces \mathbf{f}_{so} acting at DoFs o by,

$$\bar{\mathbf{f}}_{sc} = \mathbf{Y}_{sc}^{-1} \mathbf{Y}_{sco} \mathbf{f}_{so}. \quad (2)$$

Classically, direct measurement of the blocked force required the source in question to be mounted to a rigid test bench, so as to achieve the necessary constraints. In practice this condition can only be approximated over a limited frequency range. Alternatively, the blocked force can be inferred from the free source velocity through the inverse relation,

$$\bar{\mathbf{f}}_{sc} = \mathbf{Y}_{sc}^{-1} \mathbf{v}_{sc} \quad (3)$$

where; \mathbf{Y}_{sc} is the free interface mobility matrix of the source, and \mathbf{v}_{sc} is its operational free velocity, itself related to the internal generating forces by $\mathbf{v}_{sc} = \mathbf{Y}_{sco} \mathbf{f}_{so}$. However, this approach, requires the source to be operated under a freely suspended condition, which is often impractical, if not impossible.

2.1. In situ Characterisation

In work by Moorhouse et al. [11] it was shown that the blocked force may be acquired through an inverse procedure using measurements performed with the source installed on an arbitrary receiver structure. It has since been acknowledged that this phenomenon is a special case of a general theorem on the representation of fields of forced vibration in composite elastic systems [15]. In the context of structural source characterisation, the relation of note is given by [11],

$$\mathbf{v}_{cb} = \mathbf{Y}_{cb} \bar{\mathbf{f}}_{sc} \quad (4)$$

where; $\mathbf{Y}_{cb} \in \mathbb{C}^{M \times N}$ is the measured transfer mobility matrix of a coupled assembly, $\mathbf{v}_{cb} \in \mathbb{C}^M$ is a measured operational velocity vector (note that accelerance and acceleration may be used in place of mobility and velocity), and $\bar{\mathbf{f}}_{sc} \in \mathbb{C}^N$ is the vector of unknown blocked forces. Here, lower-case subscripts b and c represent remote receiver and coupling interface DoFs, respectively (see Fig. 1). Note that the DoF set b may include the interface DoFs c as a subset and that variables are represented in the frequency domain, with the frequency variable omitted for clarity. For $N = M$, providing that the measured mobility matrix is of full rank, a unique solution is found through the inverse mobility matrix $\mathbf{Y}_{cb}^{-1} = \mathbf{Z}_{cb}$, where $\mathbf{Z}_{cb} \in \mathbb{C}^{N \times N}$ is an assembly impedance matrix. For $N > M$, the pseudo-inverse may be used in place of the standard matrix inverse to obtain $\mathbf{Y}_{cb}^+ = \mathbf{Z}_{cb} \in \mathbb{C}^{M \times N}$, leading to a least squares solution of the problem.

Noting that both \mathbf{Y}_{cb} and \mathbf{v}_{cb} are properties of the coupled assembly, Eq. (4) facilitates an *in situ* determination of the blocked force, i.e. the source need not be installed on a rigid test bench and may be characterised under ‘installed’ conditions.

The experimental implementation of Eq. (4) follows a two part measurement procedure. In part 1, the source is turned off and the mobility matrix \mathbf{Y}_{cb} measured. In part 2, the source is operated and the operation velocity \mathbf{v}_{cb} measured at the chosen DoFs. The mobility \mathbf{Y}_{cb} relates the remote DoFs at which the velocity is measured to the coupling interface DoFs where the blocked force is defined. Particular care must be taken during the measurement of \mathbf{Y}_{cb} as it must be inverted numerically so as to acquire the blocked force. It is known that poor experimental data is likely to increase the chance of unacceptable errors. Although there exist numerical techniques to minimize this effect (e.g. regularisation), it is recommended that effort

be spent acquiring the best experimental data possible, as opposed to relying on such techniques. Nevertheless, even the most carefully executed experiments will be subject to some degree of uncertainty. The issue of experimental uncertainty and its propagation in a blocked force characterisation is addressed in [12].

The in situ blocked force approach, as represented by Eq. (4), has become the most promising approach towards the independent characterisation of vibratory sources. Its adoption within industry, and role in the formulation of the diagnostic procedures in situ [3] and component-based TPA [6], have led to numerous applications within the automotive [3,16,17], aerospace [18], domestic product [19,20] and building acoustics [21,22] sectors. Whilst most applications so far have involved purely experimental systems, the potentially more promising use of blocked forces is to excite numerical models directly. In either case, an awareness of the underlying assumptions and likely sources of uncertainty and error is necessary. In particular, it is the notions of *completeness* and *consistency* that are of interest here. A more detailed description of these requirements will be presented in the following section.

3. Problem statement

It has been shown that the blocked force of an active sub-structure is related to the operational response of an assembled structure through the passive dynamics of the *coupled* assembly (see Eq. (4)) [11,15]. The in situ blocked force approach treats this relation as an inverse problem, characterising the blocked force using a set of measured operational responses. Clearly, one can also consider the forward problem, i.e. predicting the operational response *due* to an applied blocked force,

$$\mathbf{p}_{Cb} = \mathbf{H}_{Cb} \bar{\mathbf{f}}_{Sc} \quad (5)$$

where \mathbf{p}_{Cb} is a response vector at the reference DoFs b , corresponding appropriately to the units of the vibro-acoustic FRF matrix \mathbf{H}_{Cb} (\mathbf{p}_{Cb} may include both structural and acoustic responses). Note that the reference DoFs b differ from those used to characterise the blocked force in Eq. (4). Using Eq. (5) the operational response of an assembled structure can be predicted so long as a) its *coupled* FRF matrix \mathbf{H}_{Cb} is known (this may, in principle, be modelled numerically, determined experimentally, or predicted using dynamic sub-structuring procedures), and b) the blocked force $\bar{\mathbf{f}}_{Sc}$ has been characterised appropriately (either in situ or on a test bench).

Together, Eqs. (4) and (5) form the basis of both in situ and component-based TPA. In an in situ TPA the forward FRF matrix \mathbf{H}_{Cb} is measured directly on the same assembly that the blocked force $\bar{\mathbf{f}}_{Sc}$ is characterised (e.g. a vehicle). Eq. (5) is then used as a diagnostic tool to determine the dominant contributions to an operational response. In a component-based TPA the forward FRF matrix \mathbf{H}_{Cb} describes some new assembly (that might not exist physically), and is predicted using, for example, dynamic sub-structuring (i.e. based on the measurement of each individual sub-structure that makes up the assembly). Eq. (5) is then used as a predictive tool, providing a response prediction in a 'virtual' assembly. We are interested generally in the conditions under which Eq. (5) provides a reliable prediction of the operational response \mathbf{p}_{Cb} .

It has been noticed in previous works [23,24] that large artefacts are observed over narrow frequency ranges in operational response predictions when transferring blocked forces from one assembly to another. We are interested in identifying the underlying cause of such artefacts, and providing appropriate measures of their severity. It will be shown through the present paper that such artefacts are related to the notions of *completeness* and *consistency*, summary descriptions of which are given below:

- *Completeness* describes the degree to which the coupling interface separating source and receiver has been correctly represented, for example whether enough DoFs have been included (i.e. rotations/in-plane). The completeness of an interface description is essential if a blocked force is to be characterised correctly and applied with confidence. The completeness of an interface description is also an essential requirement in the coupling and decoupling of sub-structures.
- *Consistency* relates to the underlying dynamics shared by the active and passive properties of an assembly or component (for example, the blocked force and free mobility of a vibration source). Consistency is a more general notion, with completeness being a special case. It arises principally when active and passive quantities are obtained from separate experiments (or potentially from experiment and numerical modelling).

The notions of completeness and consistency will be further developed through Sections 4 and 5, respectively, where appropriate measures of their severity will be introduced and numerical examples presented.

4. Completeness of an interface description

Interface completeness is a general issue encountered whenever characterisations are performed at the interface of one or more sub-structures [25]. This includes not only the characterisation of blocked forces, but also the coupling and decoupling of sub-structures. Although we will consider completeness from the perspective of a blocked force characterisation, many of the results presented may be interpreted more generally.

Conceptually, completeness can be described in simple terms with reference to Fig. 2: if all the interface DoFs (c_i and c_j) between source (S) and receiver (R) are blocked then an applied force at a will not generate a response at b ; on the other

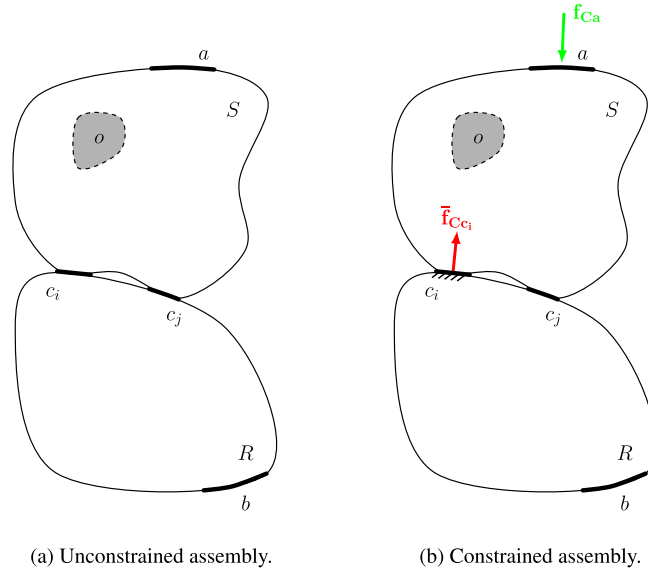


Fig. 2. Constrained and unconstrained assemblies corresponding to Eqs. (11) and (12) respectively.

hand, a finite response will be obtained if any interface DoFs (say c_j) are left unblocked. In what follows we use this fact to quantify the extent to which an interface description is complete.

We begin by considering the in situ blocked force relation Eq. (4) in the form,

$$\mathbf{v}_{Cb} = \mathbf{Y}_{Cb c_i} \bar{\mathbf{f}}_{S c_i} + \mathbf{Y}_{Cb c_j} \bar{\mathbf{f}}_{S c_j} \tag{6}$$

where the velocity contributions from known and unknown DoFs have been partitioned (see Fig. 2a). Here, c_i represents the set of coupling interface DoFs that are *known* and considered measurable, whilst c_j represents the set of interface DoFs that are physically present but have been omitted from the experimental representation of the interface, either because they are *unknown* or because they are known but cannot be measured.

In the in situ experimental determination of the blocked force one pre-multiplies the operational velocity vector by an inverse mobility matrix pertaining to the *known* DoFs, $\mathbf{Y}_{Cb c_i}^{-1}$. Pre-multiplication of Eq. (6) by $\mathbf{Y}_{Cb c_i}^{-1}$ thus yields,

$$\mathbf{Y}_{Cb c_i}^{-1} \mathbf{v}_{Cb} = \tilde{\mathbf{f}}_{C c_i} = \bar{\mathbf{f}}_{S c_i} + \mathbf{Y}_{Cb c_i}^{-1} \mathbf{Y}_{Cb c_j} \bar{\mathbf{f}}_{S c_j}. \tag{7}$$

The acquired blocked force, $\tilde{\mathbf{f}}_{C c_i}$, although correct in its own respect², is not the true blocked force at the DoFs c_i , $\bar{\mathbf{f}}_{S c_i}$. The neglect of the unknown DoFs c_j has resulted in the additional term, $\mathbf{Y}_{Cb c_i}^{-1} \mathbf{Y}_{Cb c_j} \bar{\mathbf{f}}_{S c_j}$. This term is a property of the coupled assembly and thus the acquired blocked force is no longer an independent property of the source. This loss of independence may have severe implications when the acquired blocked force is transferred to a secondary assembly and used to predict an operational response (as in Eq. (5)). This is demonstrated below.

Suppose we are interested in predicting the remote receiver velocity, \mathbf{v}_{Xb} , on a secondary assembly (denoted by the subscript, X). The true velocity (that we are aiming to predict) may be expressed in terms of the true blocked force as,

$$\mathbf{v}_{Xb} = \mathbf{Y}_{Xb c_i} \bar{\mathbf{f}}_{S c_i} + \mathbf{Y}_{Xb c_j} \bar{\mathbf{f}}_{S c_j}. \tag{8}$$

To *predict* the remote velocity the acquired blocked force, $\tilde{\mathbf{f}}_{C c_i}$, is pre-multiplied by the coupled transfer mobility of the secondary assembly that corresponds to the known and measurable DoFs, $\mathbf{Y}_{Xb c_i}$.

$$\tilde{\mathbf{v}}_{Xb} = \mathbf{Y}_{Xb c_i} \tilde{\mathbf{f}}_{C c_i} = \mathbf{Y}_{Xb c_i} \left(\bar{\mathbf{f}}_{S c_i} + \mathbf{Y}_{Cb c_i}^{-1} \mathbf{Y}_{Cb c_j} \bar{\mathbf{f}}_{S c_j} \right) \tag{9}$$

Expanding the above we arrive at,

$$\tilde{\mathbf{v}}_{Xb} = \mathbf{Y}_{Xb c_i} \bar{\mathbf{f}}_{S c_i} + \mathbf{Y}_{Xb c_i} \mathbf{Y}_{Cb c_i}^{-1} \mathbf{Y}_{Cb c_j} \bar{\mathbf{f}}_{S c_j}. \tag{10}$$

² The blocked force $\tilde{\mathbf{f}}_{C c_i}$ represents the reaction forces due to a source that is blocked in the c_i DoFs but unrestrained in the remaining c_j DoFs. It is therefore by definition a blocked force, albeit not the true blocked force.

From the above it is clear that the true velocity, $\mathbf{v}_{\mathbf{x}b}$, and the predicted velocity, $\bar{\mathbf{v}}_{\mathbf{x}b}$, are not equal. Hence the blocked force is no longer transferable. Here, the unknown blocked force, $\bar{\mathbf{f}}_{\mathbf{c}c_i}$, contributes to the predicted velocity response through the propagating transfer function, $\mathbf{Y}_{\mathbf{x}b\mathbf{c}_i}\mathbf{Y}_{\mathbf{c}b\mathbf{c}_i}^{-1}\mathbf{Y}_{\mathbf{c}b\mathbf{c}_j}$. So, whilst the response prediction still accounts for the unknown blocked force, its contribution to the response of a secondary assembly is incorrect. This discrepancy is a consequence of an incomplete interface description. Had all coupling DoFs been accounted for, the true blocked force would have been acquired, and subsequently transferred to the secondary assembly with no issues.

The notion of incompleteness may be interpreted as a form of model uncertainty [12], in the sense that the model we use to describe the problem (Eq. (4)) is incorrect (i.e. it neglects some unknown DoFs) and thus introduces an uncertainty. This uncertainty is distinct from the random uncertainty that arises due to experimental testing, instead manifesting as a systematic error. We are interested in minimising the influence of this error by quantifying whether enough DoFs have been included in an interface description. To this end, an Interface Completeness Criterion (ICC) is proposed in the following section.

4.1. Interface Completeness Criterion

In this section we will derive a criterion that quantifies the degree of completeness that an interface description possesses. The so-called *Interface Completeness Criterion* (ICC) is based on the notion of mathematically blocking the set of known DoFs at the source-receiver interface, and observing the resultant response on the receiver. Its derivation, first presented in [25], is provided below for ‘completeness’.

Consider the assembly depicted in Fig. 2a, where a source (S) and receiver (R) sub-structure are coupled via two sets of interface DoFs. Denoted c_i and c_j , these DoFs form subsets of the complete coupling interface c , such that $\{c_i \subseteq c\}$ and $\{c_j \subseteq c | c_j \cap c_i = \emptyset\}$. Also included are two sets of remote DoFs on the source and receiver. These are referred to as a and b , respectively.

The equations of motion that govern the behaviour of the coupled source-receiver assembly (as depicted in Fig. 2a) are given generally by,

$$\begin{pmatrix} \mathbf{v}_{\mathbf{C}a} \\ \mathbf{v}_{\mathbf{C}c_i} \\ \mathbf{v}_{\mathbf{C}c_j} \\ \mathbf{v}_{\mathbf{C}b} \end{pmatrix} = \begin{bmatrix} \mathbf{Y}_{\mathbf{C}aa} & \mathbf{Y}_{\mathbf{C}ac_i} & \mathbf{Y}_{\mathbf{C}ac_j} & \mathbf{Y}_{\mathbf{C}ab} \\ \mathbf{Y}_{\mathbf{C}c_i a} & \mathbf{Y}_{\mathbf{C}c_i c_i} & \mathbf{Y}_{\mathbf{C}c_i c_j} & \mathbf{Y}_{\mathbf{C}c_i b} \\ \mathbf{Y}_{\mathbf{C}c_j a} & \mathbf{Y}_{\mathbf{C}c_j c_i} & \mathbf{Y}_{\mathbf{C}c_j c_j} & \mathbf{Y}_{\mathbf{C}c_j b} \\ \mathbf{Y}_{\mathbf{C}ba} & \mathbf{Y}_{\mathbf{C}bc_i} & \mathbf{Y}_{\mathbf{C}bc_j} & \mathbf{Y}_{\mathbf{C}bb} \end{bmatrix} \begin{pmatrix} \mathbf{f}_{\mathbf{C}a} \\ \mathbf{f}_{\mathbf{C}c_i} \\ \mathbf{f}_{\mathbf{C}c_j} \\ \mathbf{f}_{\mathbf{C}b} \end{pmatrix}. \quad (11)$$

We begin by considering the case where only two external forces are applied, i.e. $\mathbf{f}_{\mathbf{C}c_i} = \mathbf{f}_{\mathbf{C}c_j} = \mathbf{0}$. The first is an arbitrary force at the remote source DoFs a , $\mathbf{f}_{\mathbf{C}a}$. The second is a constraint force at the known coupling interface DoFs c_i , $\bar{\mathbf{f}}_{\mathbf{C}c_i}$. This second force is the blocking force required to constrain the velocity $\mathbf{v}_{\mathbf{C}c_i}$ to $\mathbf{0}$. The constrained assembly may then be represented by the following set of equations,

$$\begin{pmatrix} \mathbf{v}_{\mathbf{C}a} \\ \mathbf{0} \\ \mathbf{v}_{\mathbf{C}c_j} \\ \mathbf{v}_{\mathbf{C}b} \end{pmatrix} = \begin{bmatrix} \mathbf{Y}_{\mathbf{C}aa} & \mathbf{Y}_{\mathbf{C}ac_i} & \mathbf{Y}_{\mathbf{C}ac_j} & \mathbf{Y}_{\mathbf{C}ab} \\ \mathbf{Y}_{\mathbf{C}c_i a} & \mathbf{Y}_{\mathbf{C}c_i c_i} & \mathbf{Y}_{\mathbf{C}c_i c_j} & \mathbf{Y}_{\mathbf{C}c_i b} \\ \mathbf{Y}_{\mathbf{C}c_j a} & \mathbf{Y}_{\mathbf{C}c_j c_i} & \mathbf{Y}_{\mathbf{C}c_j c_j} & \mathbf{Y}_{\mathbf{C}c_j b} \\ \mathbf{Y}_{\mathbf{C}ba} & \mathbf{Y}_{\mathbf{C}bc_i} & \mathbf{Y}_{\mathbf{C}bc_j} & \mathbf{Y}_{\mathbf{C}bb} \end{bmatrix} \begin{pmatrix} \mathbf{f}_{\mathbf{C}a} \\ \bar{\mathbf{f}}_{\mathbf{C}c_i} \\ \mathbf{0} \\ \mathbf{0} \end{pmatrix}. \quad (12)$$

The above describes an assembly that is excited by an arbitrary force at a , whilst the coupling interface, c , is *partially* constrained at the known DoFs. This constrained assembly is shown diagrammatically in Fig. 2b.

The second line of Eq. (12),

$$\mathbf{0} = \mathbf{Y}_{\mathbf{C}c_i a}\mathbf{f}_{\mathbf{C}a} + \mathbf{Y}_{\mathbf{C}c_i c_i}\bar{\mathbf{f}}_{\mathbf{C}c_i} \quad (13)$$

can be rearranged for the blocking force,

$$\bar{\mathbf{f}}_{\mathbf{C}c_i} = -\mathbf{Y}_{\mathbf{C}c_i c_i}^{-1}\mathbf{Y}_{\mathbf{C}c_i a}\mathbf{f}_{\mathbf{C}a}. \quad (14)$$

The above relation describes a force transmissibility that relates the externally applied force at a to the resultant blocking force at c_i .

The 4th line of Eq. (12), introducing the notation $\mathbf{v}_{\mathbf{C}b}^{(c_i)}$ to describe the velocity of the constrained assembly (i.e. the contribution through the unknown DoFs c_j only), gives,

$$\mathbf{v}_{\mathbf{C}b}^{(c_i)} = \mathbf{Y}_{\mathbf{C}ba}\mathbf{f}_{\mathbf{C}a} + \mathbf{Y}_{\mathbf{C}bc_j}\bar{\mathbf{f}}_{\mathbf{C}c_i}. \quad (15)$$

The first RHS term describes the velocity at b due an applied force at a on the *unconstrained* assembly, i.e. $\mathbf{v}_{\mathbf{C}b}^{(c)} = \mathbf{Y}_{\mathbf{C}ba}\mathbf{f}_{\mathbf{C}a}$. The second RHS term describes an added contribution to this velocity due to the blocking force required to constrain the interface c_i . Substituting Eq. (14) into (15) yields,

$$\mathbf{v}_{Cb}^{(c_j)} = \mathbf{Y}_{Cba} \mathbf{f}_{Ca} - \mathbf{Y}_{Cb c_i} \mathbf{Y}_{Cc_i c_i}^{-1} \mathbf{Y}_{Cc_i a} \mathbf{f}_{Ca} \tag{16}$$

or equivalently,

$$\mathbf{v}_{Cb}^{(c_j)} = \left[\mathbf{Y}_{Cba} - \mathbf{Y}_{Cb c_i} \mathbf{Y}_{Cc_i c_i}^{-1} \mathbf{Y}_{Cc_i a} \right] \mathbf{f}_a. \tag{17}$$

Eq. (17) relates an externally applied force at a to the resultant velocity at b on the constrained assembly depicted in Fig. 2b. The bracketed mobility term therefore represents the transfer mobility through the constrained assembly. Let us then define,

$$\mathbf{Y}_{Cba}^{(c_j)} \triangleq \left[\mathbf{Y}_{Cba} - \mathbf{Y}_{Cb c_i} \mathbf{Y}_{Cc_i c_i}^{-1} \mathbf{Y}_{Cc_i a} \right] \tag{18}$$

as the transfer mobility from a to b , through the DoFs c_j , whilst the DoFs c_i are blocked. Noting that the left hand term in the bracket of Eq. (17) is the transfer mobility of the unconstrained assembly, let us also define,

$$\mathbf{Y}_{Cba}^{(c)} \triangleq \mathbf{Y}_{Cba} \tag{19}$$

that is, the transfer mobility from a to b through all coupling DoFs (c_i and c_j). Finally, the right hand term in the bracket of Eq. (17) can be seen to form a round trip identity [26] for a mobility similar to \mathbf{Y}_{Cba} . It is interesting to note that for the case whereby only a single set of coupling DoFs exist, i.e. $|c_j| = 0$, this round trip identity is exactly equal to the unconstrained mobility, \mathbf{Y}_{Cba} [26]. For the constrained interface considered, however, the mobility product $\mathbf{Y}_{Cb c_i} \mathbf{Y}_{Cc_i c_i}^{-1} \mathbf{Y}_{Cc_i a}$ corresponds to a transfer mobility between a and b whilst neglecting the unknown DoFs c_j . As such, let us define,

$$\mathbf{Y}_{Cba}^{(c_i)} \triangleq \mathbf{Y}_{Cb c_i} \mathbf{Y}_{Cc_i c_i}^{-1} \mathbf{Y}_{Cc_i a}. \tag{20}$$

Using the above definitions Eq. (18) may be rewritten as,

$$\mathbf{Y}_{Cba}^{(c_j)} = \mathbf{Y}_{Cba}^{(c)} - \mathbf{Y}_{Cba}^{(c_i)} \tag{21}$$

or alternatively,

$$\mathbf{Y}_{Cba}^{(c)} = \mathbf{Y}_{Cba}^{(c_i)} + \mathbf{Y}_{Cba}^{(c_j)}. \tag{22}$$

We note here that if the DoF subset c_i contains all DoFs, $c_i = c$, then $|c_j| = 0$ and $\mathbf{Y}_{Cba}^{(c)} = \mathbf{Y}_{Cba}^{(c_i)}$. Experimentally this would mean that all of the interface DoFs have been included and the interface description is *complete*. We are therefore interested in the degree to which the equality $\mathbf{Y}_{Cba}^{(c)} = \mathbf{Y}_{Cba}^{(c_i)}$ is met.

A suitable criterion can be formulated by introducing the Cauchy–Schwarz inequality, which states that for all vectors \mathbf{x} and \mathbf{y} of an inner product space it is true that,

$$|\langle \mathbf{x}, \mathbf{y} \rangle|^2 \leq \langle \mathbf{x}, \mathbf{x} \rangle \langle \mathbf{y}, \mathbf{y} \rangle \tag{23}$$

where $\langle \cdot, \cdot \rangle$ is the inner product.³ Dividing both sides by $\langle \mathbf{x}, \mathbf{x} \rangle \langle \mathbf{y}, \mathbf{y} \rangle$ leads to the well known inequality,

$$\frac{|\langle \mathbf{x}, \mathbf{y} \rangle|^2}{\langle \mathbf{x}, \mathbf{x} \rangle \langle \mathbf{y}, \mathbf{y} \rangle} \leq 1. \tag{24}$$

We consider first the case where only a single receiver side DoF b is present. Substituting \mathbf{x} for $\mathbf{Y}_{ba}^{(c)}$ and \mathbf{y} for $\mathbf{Y}_{ba}^{(c_i)}$, whilst noting that the inner product in a complex space is obtained using the conjugate transpose^H, the *Interface Completeness Criterion* (ICC) is defined as,

$$ICC_{ba} = \frac{\left| \mathbf{Y}_{Cba}^{(c)} \left(\mathbf{Y}_{Cba}^{(c_i)} \right)^H \right|^2}{\mathbf{Y}_{Cba}^{(c)} \left(\mathbf{Y}_{Cba}^{(c)} \right)^H \mathbf{Y}_{Cba}^{(c_i)} \left(\mathbf{Y}_{Cba}^{(c_i)} \right)^H} \tag{25}$$

where: $\mathbf{Y}_{Cba}^{(c)}$ represents the directly measured transfer mobility between the source side DoFs a and the (single) receiver side DoF b , and $\mathbf{Y}_{Cba}^{(c_i)} = \mathbf{Y}_{Cb c_i} \mathbf{Y}_{Cc_i c_i}^{-1} \mathbf{Y}_{Cc_i a}$ describes the same mobility but *reconstructed* through the known interface DoFs.

Note that $\mathbf{Y}_{Cb c_i}$, $\mathbf{Y}_{Cc_i c_i}$ and $\mathbf{Y}_{Cc_i a}$ are all measurable and, provided that the source is reasonably accessible so that excitations can be applied at a and c_i , require little additional effort over and above what would be required as part of a standard blocked force characterisation. If access is restricted, and only remote measurements are available, an alternative approach may be required.

Although the source side DoFs (a) are unlikely to coincide with the true excitation DoFs of the source (o) this is not an issue, so long as the chosen set of DoFs are able to excite all interface modes. To achieve this it is recommended that multiple

³ This is the same inequality from which the Modal Assurance Criterion (MAC) is formulated.

excitations be applied in different directions. The specific number of excitations required will likely vary from case to case, and is subject to further investigation.

The ICC as defined in Eq. (25) considers only a single receiver side DoF b [25]. In the case that multiple DoFs are of interest, the *vectorised* mobilities,

$$\mathbf{Y}_{\text{Cba}}^{(c)} = \left[\mathbf{Y}_{\text{Cb}_1\text{a}}^{(c)}, \mathbf{Y}_{\text{Cb}_2\text{a}}^{(c)}, \dots, \mathbf{Y}_{\text{Cb}_n\text{a}}^{(c)} \right] \quad (26)$$

and

$$\mathbf{Y}_{\text{Cba}}^{(c_i)} = \left[\mathbf{Y}_{\text{Cb}_1\text{a}}^{(c_i)}, \mathbf{Y}_{\text{Cb}_2\text{a}}^{(c_i)}, \dots, \mathbf{Y}_{\text{Cb}_n\text{a}}^{(c_i)} \right] \quad (27)$$

may be used in place of $\mathbf{Y}_{\text{Cba}}^{(c)}$ and $\mathbf{Y}_{\text{Cba}}^{(c_i)}$, respectively. This combined ICC accounts for all receiver side DoFs.

If all coupling DoFs are accounted for, that is, $c_i = c$, the ICC is equal to one. Similarly, if $|c_i| < |c|$ then the ICC is less than 1. If none of the coupling DoFs are accounted for, that is, $|c_i| = 0$, the ICC is undefined, since $\mathbf{Y}_{\text{Cba}}^{(c_i)}$ can not be calculated. In practice, it is important to note that the mobilities used as part of Eq. (25) are obtained from measurement. As such, they are subject to some degree of uncertainty and, even in the case of a complete interface description, an ICC equal to 1 is unlikely to be achieved.

As a final remark, it should be noted that the ICC may also be applied in the case of sub-structure decoupling to assess the completeness of the interface description used.

4.2. Numerical example – Discretisation of a continuous interface

In this numerical example the Interface Completeness Criterion (ICC) is used to assess the completeness of a discrete approximation to a continuous interface. The interface considered is an arbitrary line that separates two sides of a simply supported rectangular plate, as illustrated in Fig. 3. Interfaces of this type are often encountered in practical scenarios, for example when vibratory sources are welded to their receiver structure, and are typically represented by a series of discrete point-like DoFs. It is the aim of this study to investigate the degree to which this approximation accounts for the continuous nature of the interface. This will be done by computing the ICC for increasing levels of its discretisation.

The left hand side of the interface is considered a source sub-structure, and the right hand side the receiver sub-structure. The coupled plate assembly is modelled analytically using a truncated modal summation. Note that only the translational z and rotational α and β DoFs (i.e. those around the x and y axis) are accounted for. The geometric and material properties of the model are given in Table 1.

The continuous interface that separates the source and receiver is described by an increasing number of points, as illustrated in Fig. 4. Here, each point-like DoF, unless otherwise specified, includes three *coordinate*-DoFs: z , α and β . As shown in Fig. 3, a further five points were chosen on the source side (a) along with a single point on the receiver side (b).

The ICC between the 15 source side DoFs and each of the 3 receiver side DoFs (denoted, ICC_{za} , $\text{ICC}_{\alpha a}$ and $\text{ICC}_{\beta a}$) are calculated as per Eq. (25). Also calculated is the *combined* ICC, obtained by vectorising the appropriate mobilities, as discussed in Section 4.1. Six interface descriptions are considered here, corresponding to 2, 3, 4, 5, 10 and 20 points, evenly spread across the breadth of the plate, as illustrated through Figs. 4a–f, respectively. The corresponding ICCs are shown in Fig. 5, where those pertaining to the translational and rotational (α and β) receiver DoFs are shown in grey and indicated by triangular, circular and square markers, respectively. Shown in black are the combined ICCs, i.e. those determined by vectorising the mobilities as per Eqs. (26) and (27).

Fig. 5 clearly illustrates that an increase in the number of DoFs used to describe the continuous interface leads to a convergence of the ICC to 1. Whilst this convergence is observed for each coordinate-DoF, it can be seen that their respective ICCs tend to differ from one another. This supports the use of a combined ICC, which provides a more general overall trend between the three receiver side DoFs.

Shown in Fig. 6 are two combined ICCs corresponding to an interface description made up of 20 points with and without rotational DoFs. In Fig. 6a the coupling interface description includes both translational and rotational coordinate-DoFs (as in Fig. 4f). In Fig. 6b the coupling interface description includes only translational coordinate-DoFs, i.e. the rotational DoFs were neglected. As one might expect, the neglect of rotational coupling has resulted in a worsening of the ICC. Whilst this is an intuitively obvious result, it highlights the importance of rotational DoFs in the description of a continuous interface and, furthermore, the ability of the ICC to quantify it.

Although only a simple numerical study, the above demonstrates the application of the ICC to quantify the completeness of an interface description and illustrates some example results for a continuous interface. An experimental application of the ICC will be presented later in Section 6 as part of an experimental study. Further experimental applications of the ICC can be found in [17,25,27].

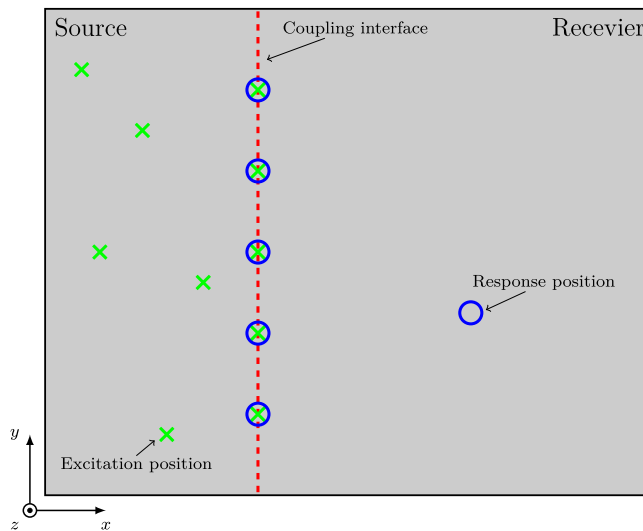


Fig. 3. Diagrammatic representation of the continuous interface numerical study. Two plates are coupled via a continuous interface (dashed red line) in the translational z and x/y rotational DoFs, α and β . Green crosses correspond to positions that require excitations to be applied, and blue circles to those that require responses to be measured. (For interpretation of the references to colour in this figure, the reader is referred to the web version of this article.)

Table 1

Geometry of the coupled plate assembly, plate 1 and plate 2. The material properties of the three plates are; Young's modulus $E = 200 \times 10^9$ [N/m²], density $\rho = 9000$ [kg/m³], Poisson's ratio $\mu = 0.3$, and loss factor $\eta = 0.1$.

Plate	Dimensions (x × y × z) [m]
Coupled	1 × 0.8 × 0.005
Source	0.35 × 0.8 × 0.005
Receiver	0.65 × 0.8 × 0.005

5. Consistency between active and passive properties

In Section 4 it was shown that the neglect of interface DoFs when characterising the blocked force, referred to here as incompleteness, can lead to systematic errors in the predicted response of an assembly. In this section it will be shown that further errors arise when the acquired blocked force is *inconsistent* with the passive properties of the assembly.

The issue of inconsistency can be illustrated diagrammatically using Fig. 7. Suppose the blocked force of a vibration source is obtained from an assembly C (Fig. 7a). Whilst the source is attached and/or operational its dynamic properties are altered, for example a stiffening may occur due to an operational load. This altered source is denoted S' with the corresponding blocked force $\bar{f}_{S'c}$. The vibration source is then detached and its free mobility Y_{Sc} is measured (or perhaps modelled numerically). In this free state the source dynamics are no longer influenced by coupling, nor its operational state. The free source mobility is then used to predict the coupled mobility of a new assembly X (Fig. 7b). Although valid in their own right, the passive source properties of this assembly are inconsistent with those of the blocked force, $S \neq S'$. When the blocked force is used to predict the operational response of assembly X, the inconsistency $S \neq S'$ can lead to artefacts in the response prediction.

Clearly the issue of inconsistency is a very general one, the above demonstrating just one example, with many others possible. To investigate the underlying cause of inconsistency we will begin by considering a simplified mass-spring model before presenting a more general treatment for arbitrary structures.

5.1. Simplified example

To clearly understand the nature of inconsistency we will first consider a simplified system composed of a mass-spring element (source) coupled to an arbitrary structure (receiver) represented by the dynamic stiffness D , as illustrated in Fig. 8. It will be shown that when a coupled FRF and blocked force are combined, there is a cancellation of terms between the two. If the coupled FRF and blocked force are obtained from separate tests it is likely that these cancelling terms will not be identical (they will be inconsistent), and an artefact will remain.

Assuming harmonic excitation with time dependence $e^{i\omega t}$, the equations of motion for the mass-spring system are given by,

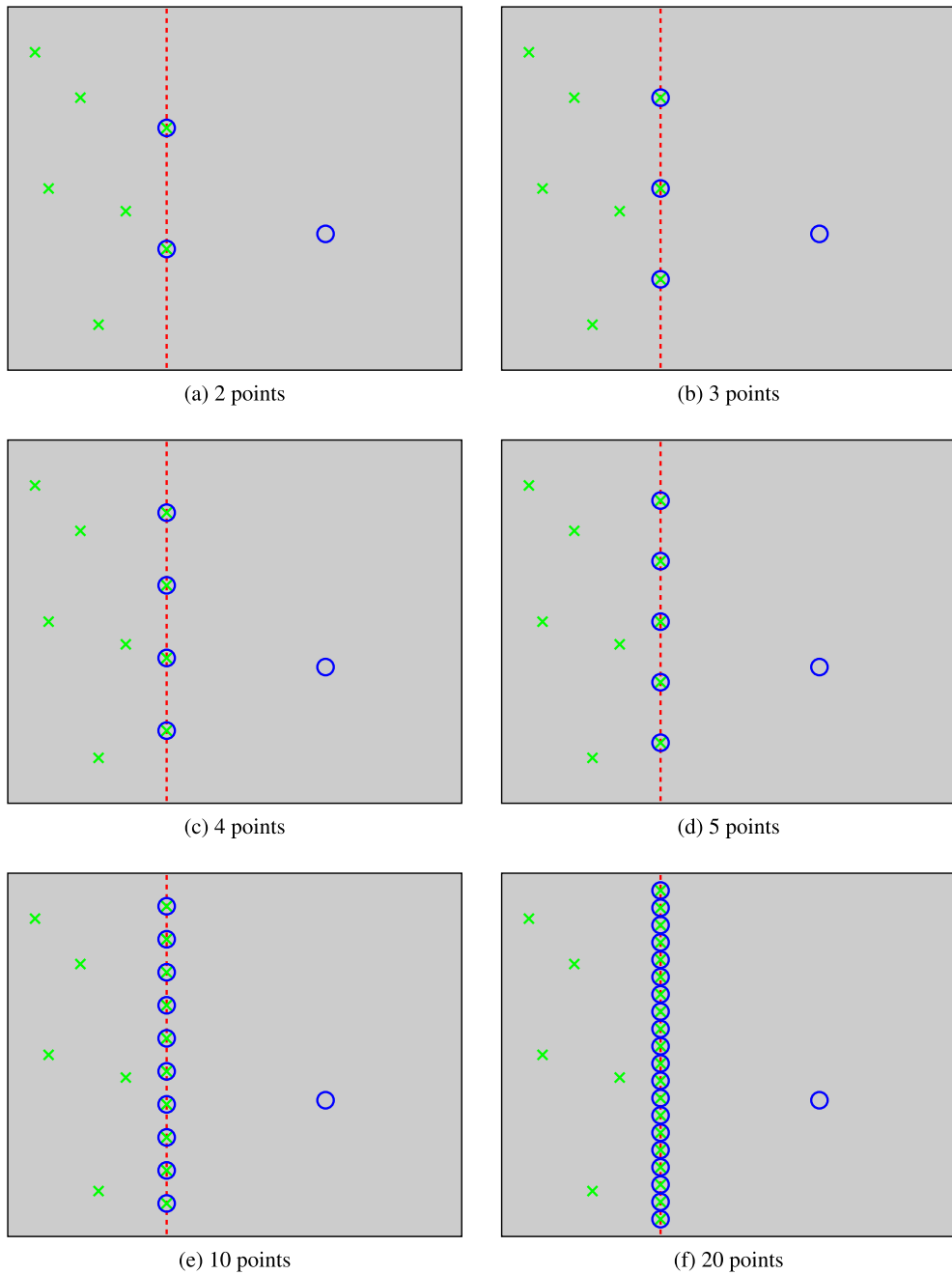


Fig. 4. Diagrammatic representation of the continuous interface numerical study. Two plates are coupled via a continuous interface which is approximated through varying degrees of discretisation. Green crosses correspond to positions that require excitations to be applied, and blue circles to those that require responses to be measured. (For interpretation of the references to colour in this figure, the reader is referred to the web version of this article.)

$$M\ddot{x}_1 + C(\dot{x}_1 - \dot{x}_2) + K(x_1 - x_2) = F_1 \quad (28)$$

$$Dx_2 + C(\dot{x}_2 - \dot{x}_1) + K(x_2 - x_1) = 0. \quad (29)$$

The response displacements due to the applied load F_1 can be obtained by inverting Eqs. 28–29,

$$\begin{pmatrix} x_1 \\ x_2 \end{pmatrix} = \frac{1}{\det[\]} \begin{bmatrix} D + i\omega C + K & i\omega C + K \\ i\omega C + K & -\omega^2 M + i\omega C + K \end{bmatrix} \begin{pmatrix} F_1 \\ 0 \end{pmatrix} \quad (30)$$

where, $\det[\] = (D - \omega^2 M)(i\omega C + K) - (i\omega C + K)^2$. Consequently the response x_2 due to the applied load F_1 is given by,

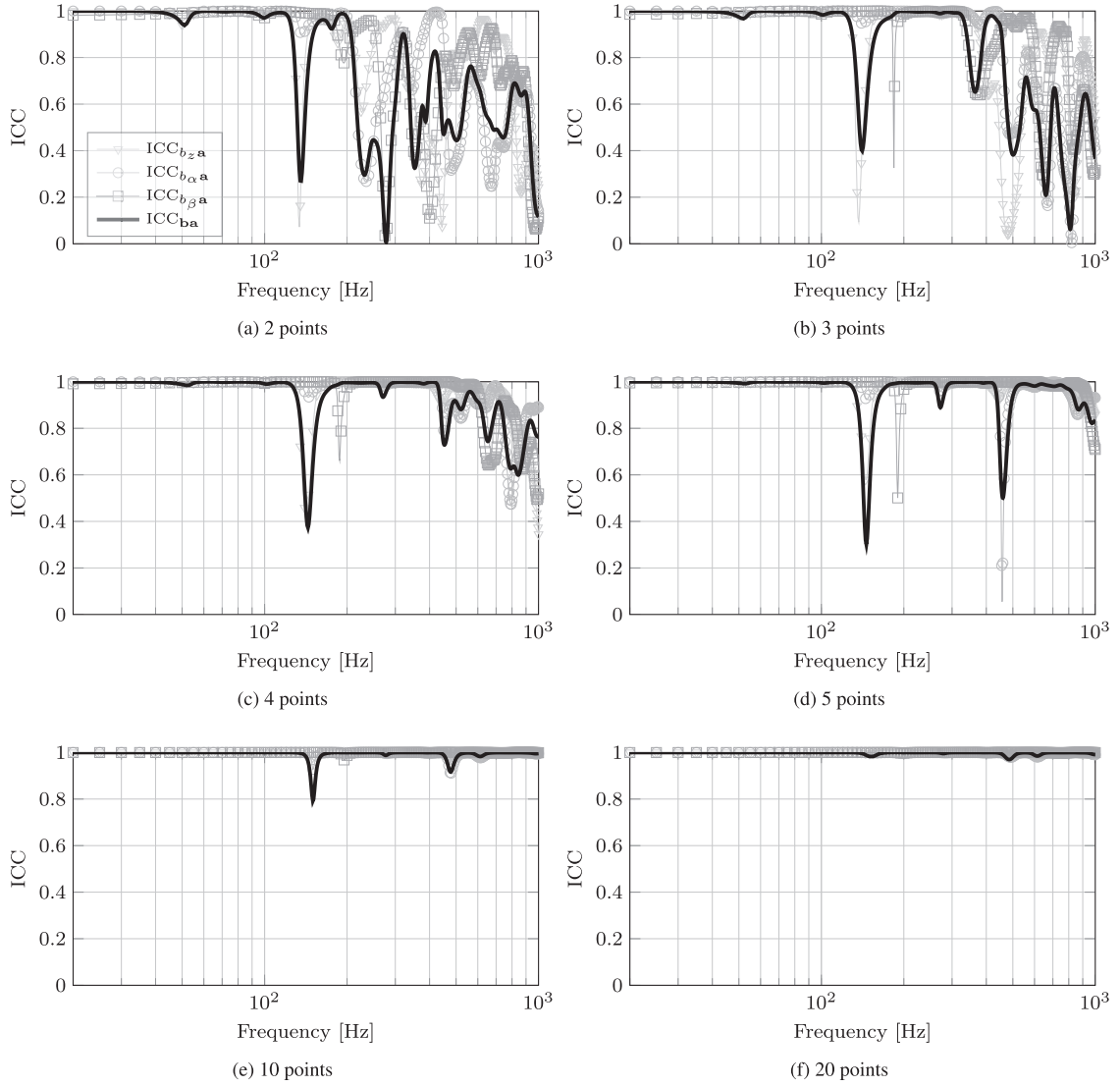


Fig. 5. Interface Completeness Criteria (ICC) for a continuous interface approximated using six different levels of discretisation (see Fig. 4). From (a) to (f), the interface is represented by 2, 3, 4, 5, 10 and 20 points, each of which includes translational z and rotational α and β DoFs (i.e. those around the x and y axis). The combined ICC (in black) is calculated using 15 source side DoFs (including z , α and β at each) and three receiver side DoFs (including z , α and β).

$$x_2 = \frac{i\omega C + K}{\det[\quad]} F_1. \tag{31}$$

By setting $x_2 = 0$ in Eq. (30) and rearranging the bottom row the blocked force of the mass-spring element is found as,

$$\bar{F}_2 = \frac{-(i\omega C + K)}{-\omega^2 M + i\omega C + K} F_1. \tag{32}$$

In an experimental setting this blocked force would be obtained using the in situ characterisation procedure.

According to the blocked force theory outlined above, the response obtained (downstream of the interface) when the negative blocked force is applied to the interface, in absence of the original load F_1 , is identical to that of the original loading. Substitution of Eq. (32) into Eq. (30) (setting $F_1 = 0$) yields,

$$\begin{pmatrix} x_1 \\ x_2 \end{pmatrix} = \frac{1}{\det[\quad]} \begin{bmatrix} D + i\omega C + K & i\omega C + K \\ i\omega C + K & -\omega^2 M + i\omega C + K \end{bmatrix} \begin{pmatrix} 0 \\ \frac{-i\omega C + K}{-\omega^2 M + i\omega C + K} F_1 \end{pmatrix} \tag{33}$$

from which,

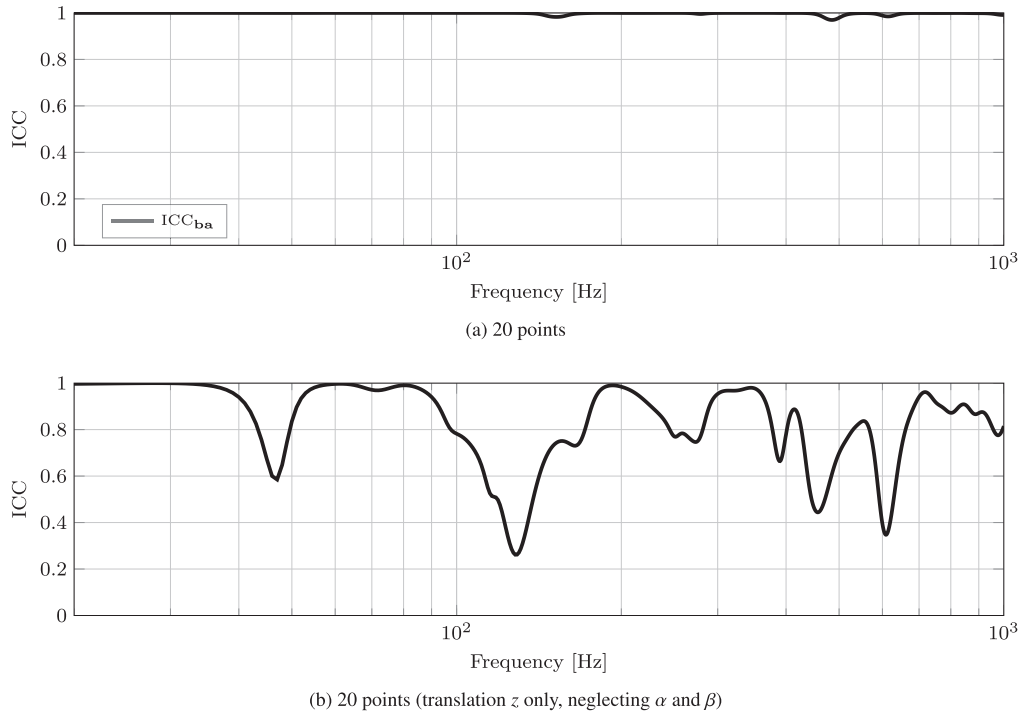


Fig. 6. Interface Completeness Criteria (ICC) for a continuous interface approximated using 20 points, both with (a) and without (b) rotational coupling. The ICC is calculated using 15 source side DoFs (including z , α and β at each) and three receiver side DoFs (including z , α and β). Only the combined ICC is shown for clarity.

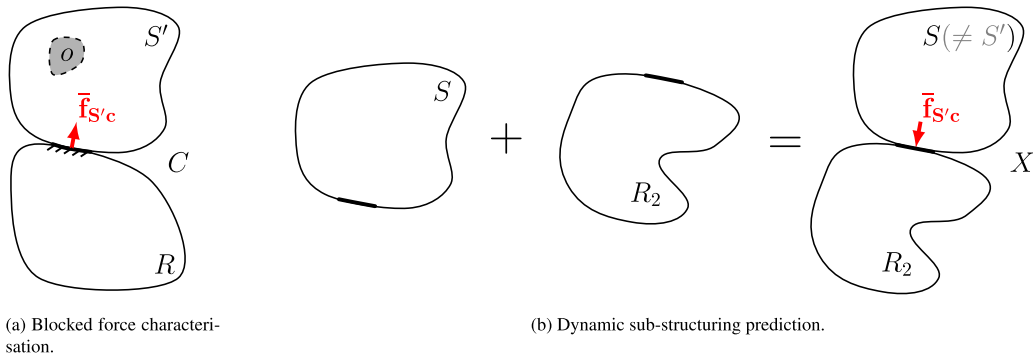


Fig. 7. Illustrative example of inconsistency.

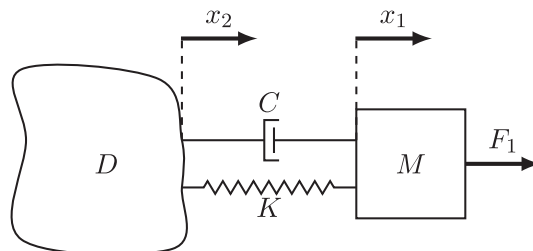


Fig. 8. Illustration of the mass-spring system used in simplified example of inconsistency.

$$x_2 = \frac{-\omega^2 M + i\omega C + K}{\det[\quad]} \left(\frac{i\omega C + K}{-\omega^2 M + i\omega C + K} F_1 \right). \quad (34)$$

The first term on the right hand side is the coupled receptance of the mass-spring system. In an experimental setting this would be measured (or modelled) as part of some secondary FRF test, separate to the blocked force characterisation.

It is clear from the above that a cancellation occurs between the denominator of the blocked force and the numerator of the coupled receptance. The roots of the denominator describe the blocked modes of the source sub-structure. The above can therefore be interpreted as a cancellation of blocked modes. An inconsistency between the two, due to them being obtained from separate tests for example, will lead to an imperfect cancellation and artefacts in the response x_2 .

5.2. General formulation

We will now consider inconsistency more generally for arbitrary source and receiver structures. Suppose the blocked force $\tilde{\mathbf{f}}_{\text{Sc}}$ is acquired from some assembly C (assuming, for now, a complete interface description),

$$\tilde{\mathbf{f}}_{\text{Sc}} = \mathbf{Y}_{\text{Ccc}}^{-1} \mathbf{v}_{\text{Cc}}, \quad (35)$$

where $\tilde{\cdot}$ is used to denote an in situ measured blocked force. The measured velocity \mathbf{v}_{Cc} can be substituted for the product of the *true* blocked force and the coupled mobility as so,

$$\tilde{\mathbf{f}}_{\text{Sc}} = \mathbf{Y}_{\text{Ccc}}^{-1} (\mathbf{Y}_{\text{Ccc}} \tilde{\mathbf{f}}_{\text{Sc}}). \quad (36)$$

Similarly, the true blocked force can be substituted for the *internal* generating force \mathbf{f}_{So} ,

$$\tilde{\mathbf{f}}_{\text{Sc}} = \mathbf{Y}_{\text{Ccc}}^{-1} (\mathbf{Y}_{\text{Ccc}} \mathbf{Y}_{\text{Scc}}^{-1} \mathbf{Y}_{\text{Scc}} \mathbf{f}_{\text{So}}). \quad (37)$$

Using the measured blocked force $\tilde{\mathbf{f}}_{\text{Sc}}$ we can predict the operational response in a new assembly X as per Eq. 5,

$$\mathbf{p}_{\text{Xb}} = \mathbf{H}_{\text{Xbc}} \tilde{\mathbf{f}}_{\text{Sc}}. \quad (38)$$

The assembled structure's FRF \mathbf{H}_{Xbc} can be expressed in terms of the uncoupled source and receiver FRFs (assumed to be measured separately),

$$\mathbf{H}_{\text{Xbc}} = \mathbf{H}_{\text{Rbc}} (\mathbf{Y}_{\text{Scc}} + \mathbf{Y}_{\text{Rcc}})^{-1} \mathbf{Y}_{\text{Scc}}. \quad (39)$$

Now substituting Eqs. (37) and (39) into (38), whilst denoting those quantities that are measured directly with the superscript ^m, we obtain an expression for the operational response at *b* in the assembly X, in terms of the internal excitation at *o*,

$$\mathbf{p}_{\text{Xb}} = \left[\mathbf{H}_{\text{Rbc}}^{\text{m}} (\mathbf{Y}_{\text{Scc}}^{\text{m}} + \mathbf{Y}_{\text{Rcc}}^{\text{m}})^{-1} \mathbf{Y}_{\text{Scc}}^{\text{m}} \right] (\mathbf{Y}_{\text{Ccc}}^{\text{m}})^{-1} (\mathbf{Y}_{\text{Ccc}} \mathbf{Y}_{\text{Scc}}^{-1} \mathbf{Y}_{\text{Scc}} \mathbf{f}_{\text{So}})^{\text{m}}. \quad (40)$$

The notion of consistency is introduced by simply acknowledging the cancellation of \mathbf{Y}_{Ccc} and \mathbf{Y}_{Scc} , which leads to,

$$\mathbf{p}_{\text{Xb}} = \mathbf{H}_{\text{Rbc}} (\mathbf{Y}_{\text{Scc}} + \mathbf{Y}_{\text{Rcc}})^{-1} \mathbf{Y}_{\text{Scc}} \mathbf{f}_{\text{So}}. \quad (41)$$

Eq. (41) represents the true response at *b* given the initial excitation \mathbf{f}_{So} . It is clear from the above that the necessary cancellations will only occur if the mobility matrices $\mathbf{Y}_{\text{Scc}}^{\text{m}}$ and $\mathbf{Y}_{\text{Ccc}}^{\text{m}}$ are in exact agreement with those contained *within* the operational velocity, $\mathbf{v}_{\text{Cc}} = (\mathbf{Y}_{\text{Ccc}} \mathbf{Y}_{\text{Scc}}^{-1} \mathbf{Y}_{\text{Scc}} \mathbf{f}_{\text{So}})^{\text{m}}$.

The initial cancellation of $\mathbf{Y}_{\text{Ccc}}^{\text{m}}$ can be interpreted as removing the effect of the assembly in which the blocked force was characterised. As illustrated in Section 4, this requires a complete interface description. Any incompleteness in the characterisation of the blocked force will lead to an improper cancellation of $\mathbf{Y}_{\text{Ccc}}^{\text{m}}$ and the introduction of an inconsistency. Note that any change in the passive properties of assembly C between the active (whilst measuring \mathbf{v}_{Cc}) and passive (whilst measuring \mathbf{Y}_{Ccc}) test phases, e.g. due to an applied torque or stiffening effect when under operation, will also introduce an inconsistency, even in the presence of a complete interface description.

The cancellation of the free source mobility $\mathbf{Y}_{\text{Scc}}^{\text{m}}$ can be interpreted, as in Section 5.1, as a cancellation of blocked interface modes. Additional inconsistencies may arise here if the free mobility is not representative of the source, for example if a 'free' boundary condition is not achieved during its measurement or if the source's passive properties change when operational.

Whilst the mobility $\mathbf{Y}_{\text{Ccc}}^{\text{m}}$ is measured as part of the blocked force characterisation, in a component-based TPA the source mobility $\mathbf{Y}_{\text{Scc}}^{\text{m}}$ may be measured or modelled. In the context of a Digital Twin, a modelled source mobility may prove more advantageous, in which case there is even greater potential for an inconsistency between modelled and measured properties.

Note that one can envisage other causes of inconsistency besides those discussed above. For example, due to a change in the excitation mechanism between coupled and uncoupled states, experimental error in the measurement of FRFs (of both measurement and operator origins [28]), non-linearity in the passive properties of the source, or a change in environmental conditions (e.g. temperature/humidity), to name but a few.

Like incompleteness, inconsistency may be interpreted as a form of model uncertainty [12], manifesting as a systematic error. We are interested in quantifying the effect of inconsistency so as to indicate the reliability of an operational response prediction. To this end, a Measurement Consistency Criterion (MCC) is proposed in the following section.

5.3. Measurement Consistency Criterion

In this section we will derive a criterion that quantifies the consistency between the blocked force and free mobility of a vibration source. The consistency between other active/passive quantities, such as the coupled mobility and operational velocity (as used in a blocked force characterisation), is subject to further investigation.

The *Measurement Consistency Criterion* (MCC) is formulated by first establishing an equality that is met only when consistency is achieved. From Eq. (40) an appropriate equality is given by,⁴

$$\mathbf{Y}_{\text{Scc}}^{\text{m}} (\mathbf{Y}_{\text{Ccc}}^{\text{m}})^{-1} (\mathbf{Y}_{\text{Ccc}} \mathbf{Y}_{\text{Scc}}^{-1} \mathbf{Y}_{\text{Scc}} \mathbf{f}_{\text{So}})^{\text{m}} \stackrel{?}{=} (\mathbf{Y}_{\text{Scc}} \mathbf{f}_{\text{So}})^{\text{m}}. \quad (42)$$

Note that the RHS of Eq. (42) is the directly measured free velocity, $\mathbf{v}_{\text{Sc}}^{\text{m}}$, and that the LHS is a predicted free velocity using the inversely determined blocked force (see Eq. (3)), $\mathbf{v}_{\text{Sc}}^{\text{p}}$. This equality can then be rewritten as,

$$\mathbf{v}_{\text{Sc}}^{\text{p}} \stackrel{?}{=} \mathbf{v}_{\text{Sc}}^{\text{m}}. \quad (43)$$

Eq. (43) states that the blocked force and free mobility are consistent only if they are able to correctly predict the true free velocity of the source. A measure of consistency can thus be obtained by comparing the ‘similarity’ of these two free velocity vectors.

Using the Cauchy–Schwarz inequality, the Measurement Consistency Criterion (MCC) is defined as,

$$\text{MCC}_{\text{c}} = \frac{|\langle \mathbf{v}_{\text{Sc}}^{\text{p}}, \mathbf{v}_{\text{Sc}}^{\text{m}} \rangle|^2}{(\mathbf{v}_{\text{Sc}}^{\text{p}})^{\text{H}} \mathbf{v}_{\text{Sc}}^{\text{p}} (\mathbf{v}_{\text{Sc}}^{\text{m}})^{\text{H}} \mathbf{v}_{\text{Sc}}^{\text{m}}} \quad (44)$$

where $\mathbf{v}_{\text{Sc}}^{\text{m}}$ is the directly *measured* free velocity, and $\mathbf{v}_{\text{Sc}}^{\text{p}} = \mathbf{Y}_{\text{Scc}} \tilde{\mathbf{f}}_{\text{Sc}}$ is the free velocity *predicted* using the acquired blocked force.

Note that Eq. (44) requires a direct measurement of the free velocity. This is often not possible, for example if the source has to be loaded in some way to operate. In this case an alternative MCC can be defined using artificial excitations in place of an operational activity.

To formulate a *passive* MCC, i.e. using artificial excitations, we note that the free velocity due to an artificial unit excitation is simply the transfer mobility from the (single) excitation position a to the interface DoFs c , $\mathbf{v}_{\text{Sc}} \rightarrow \mathbf{Y}_{\text{Sca}}$. A passive MCC can therefore be formulated in terms of mobilities alone.

As with the ICC, these artificial excitations should be representative of the source’s operational state, that is, they should excite the same interface modes. This may be achieved by applying multiple excitations to the source in different directions.⁵

By doing so the vectorised mobility $\mathbf{Y}_{\text{Sca}}^{\text{m}} = [\mathbf{Y}_{\text{Sca}_1}^{\text{m}}, \mathbf{Y}_{\text{Sca}_2}^{\text{m}}, \dots, \mathbf{Y}_{\text{Sca}_n}^{\text{m}}]^{\text{T}}$ may be formed. These excitations are repeated whilst the source is installed and used to determine a (normalised) blocked force (this is done by replacing the operational velocity \mathbf{v}_{Cc} with the mobility \mathbf{Y}_{Cca} in the blocked force calculation). Using the normalised blocked force we are able to predict a set of (normalised) free velocities. These correspond to the mobilities $\mathbf{Y}_{\text{Sca}}^{\text{p}} = [\mathbf{Y}_{\text{Sca}_1}^{\text{p}}, \mathbf{Y}_{\text{Sca}_2}^{\text{p}}, \dots, \mathbf{Y}_{\text{Sca}_n}^{\text{p}}]^{\text{T}}$, where $\mathbf{Y}_{\text{Sca}_i}^{\text{p}} = \mathbf{Y}_{\text{Scc}} \mathbf{Y}_{\text{Ccc}}^{-1} \mathbf{Y}_{\text{Cca}_i}$. For an artificial excitation, the passive MCC is then given by,

$$\text{MCC}_{\text{ca}} = \frac{|\langle \mathbf{Y}_{\text{Sca}}^{\text{p}}, \mathbf{Y}_{\text{Sca}}^{\text{m}} \rangle|^2}{(\mathbf{Y}_{\text{Sca}}^{\text{p}})^{\text{H}} \mathbf{Y}_{\text{Sca}}^{\text{p}} (\mathbf{Y}_{\text{Sca}}^{\text{m}})^{\text{H}} \mathbf{Y}_{\text{Sca}}^{\text{m}}}. \quad (45)$$

Like the ICC, the MCC is a scalar value bound between 0 and 1. Consistency is indicated by an MCC of 1. A value less than one indicates some form of inconsistency. It is important to note that the MCC, although able to indicate the presence of an inconsistency, is unable to indicate its precise origin (e.g. whether it’s due to a change in the passive properties whilst under operation or simply an experimental error). If, however, an ICC is available from the blocked force characterisation, this may be used to indicate whether or not the inconsistency is due to an incompleteness.

⁴ Pre-multiplying both sides of Eq. (42) by $\mathbf{Y}_{\text{Scc}}^{\text{m}}$ would yield an alternative equality. In this case, the left-hand side would represent the blocked force acquired through the in situ procedure, and the right-hand side the blocked force determined using the free source mobility and the free velocity. As in Eq. (40), an equality between the two would indicate a consistency between the blocked force and free source mobility.

⁵ Note that by using artificial excitations it is not possible to identify inconsistencies that arise due to a change in the passive properties of the source whilst under operation.

5.4. Numerical example – Coupled plate model

In this numerical example the Measurement Consistency Criterion (MCC) is used to assess the consistency between the blocked force and free mobility of a source sub-structure. Shown in Fig. 9 is an illustration of the model considered. Two FE plates (modelled using HTK thick plate elements [29]) are rigidly coupled (in z , α and β coordinate-DoFs) at 4 points (c). An additional remote DoF is included on both source (a) and receiver (b) sub-structures. Plate geometry and material properties are given in Table 2.

With the aim of identifying inconsistencies between the blocked force and free mobility, two cases will be considered here. In the first, an inconsistency is introduced through the blocked force, which is determined using an incomplete interface description. This sort of inconsistency would be encountered in practice if, for example, some important DoFs were not included in the interface description. In the second, an inconsistency is introduced through the free source mobility by perturbing the 1st, 2nd and 4th natural frequencies of the uncoupled source plate. This sort of inconsistency would be encountered in practice if, for example, the passive properties of the source changed when installed, or if the source mobility were modelled numerically and differed from its true value.

5.4.1. Case 1 – Blocked force inconsistency

Often in an experimental setting it is not possible to measure the rotational (or in-plane) DoFs necessary for a complete interface description. This incompleteness introduces an inconsistency between the blocked force and the free source mobility. In this first example the rotational β DoF at a single coupling interface has been neglected when determining the blocked force. Shown in Fig. 10a are the translational z blocked forces at an interface point for the complete (true) and incomplete (predicted) interface descriptions. It is clear that the neglect of a rotational β DoF introduces an error in the blocked force, as discussed in Section 4, the severity of which appears to increase with frequency.

The incomplete blocked force is subsequently used to predict the free source velocity in the retained DoFs, an example of which is shown in Fig. 10b. The effect of the incomplete interface description is evident here, particularly in the region of 600–1000 Hz, where large deviations are observed against the true free velocity.

Having predicted the free velocity using the incomplete blocked force and the (true) free source mobility, the MCC can be calculated and used to indicate regions of inconsistency. Shown in Fig. 10c are the MCCs calculated for each excitation DoF, z , α and β , denoted by triangular, circular and rectangular markers, respectively. Also shown is the combined MCC, obtained by vectorising the free velocities due to each excitation. The MCC clearly indicates large regions of inconsistency, particularly above 600 Hz. This is in agreement with the discrepancies observed when the incomplete blocked force is used to predict a remote response in the receiver (at DoF b), as illustrated in Fig. 10d. The results presented in Fig. 10 suggest that the MCC is capable of identifying the frequency range over which unreliable predictions are likely to be obtained. In practice, this may allow for artefacts to be identified and distinguished from physical features in a response prediction, or to indicate over which frequency range a response prediction should be considered with care.

5.4.2. Case 2 – Free mobility inconsistency

In this second example we introduce an inconsistency through the free source mobility by perturbing the natural frequency and damping of the uncoupled source's 1st, 2nd and 4th bending modes. This sort of discrepancy may occur if, for example, the passive properties of the source changed when installed, or if the source mobility were modelled numerically.

Shown in Fig. 11a are the point mobilities at an interface DoF for the true and perturbed source.⁶ Using the perturbed source mobility and the *true* blocked force, a free velocity prediction is obtained, an example of which is shown in Fig. 11b. Also shown in Fig. 11b are the true and perturbed free velocities obtained directly. Using the predicted and perturbed free source velocity we can calculate the MCC for each excitation DoF; z , α and β , the results of which are shown in Fig. 11c. Also shown is the combined MCC, obtained by vectorising the free velocities due to each excitation. The perturbed free velocity is used to calculate the MCC as in practice the free velocity would be obtained from the same experiment as the free mobility, and therefore subject to the same inconsistency.

Note that the MCC does not indicate any inconsistency in the region 200–300 Hz and 600 Hz, where the perturbations are greatest. This is expected as the perturbed source is used to obtain both the direct and predicted free velocity (its prediction involves the free mobility, which is perturbed by the same amount as the free velocity). The effect of the perturbation effectively cancels (the perturbed and predicted free velocities in Fig. 11b are in good agreement about the resonance). With reference to Eq. 42,

$$\mathbf{Y}_{\text{Scc}}^{\text{m}} (\mathbf{Y}_{\text{Dcc}}^{\text{m}})^{-1} (\mathbf{Y}_{\text{Dcc}} \mathbf{Y}_{\text{Scc}}^{-1} \mathbf{Y}_{\text{Scc}} \mathbf{f}_{\text{So}})^{\text{m}} = (\mathbf{Y}_{\text{Scc}} \mathbf{f}_{\text{So}})^{\text{m}} \quad (46)$$

$\mathbf{Y}_{\text{Scc}}^{\text{m}}$ and $\mathbf{v}_{\text{Sc}} = (\mathbf{Y}_{\text{Scc}} \mathbf{f}_{\text{So}})^{\text{m}}$ are both affected by the same perturbation, and therefore consistent with one another. The source mobilities within the *coupled* velocity term $\mathbf{v}_{\text{Cc}} = (\mathbf{Y}_{\text{Dcc}} \mathbf{Y}_{\text{Scc}}^{-1} \mathbf{Y}_{\text{Scc}} \mathbf{f}_{\text{So}})^{\text{m}}$ however, are not. This is the inconsistency indicated by

⁶ Note that a third bending mode occurs at approx. 575 Hz, but does not contribute to the displayed FRF, and is therefore not visible.

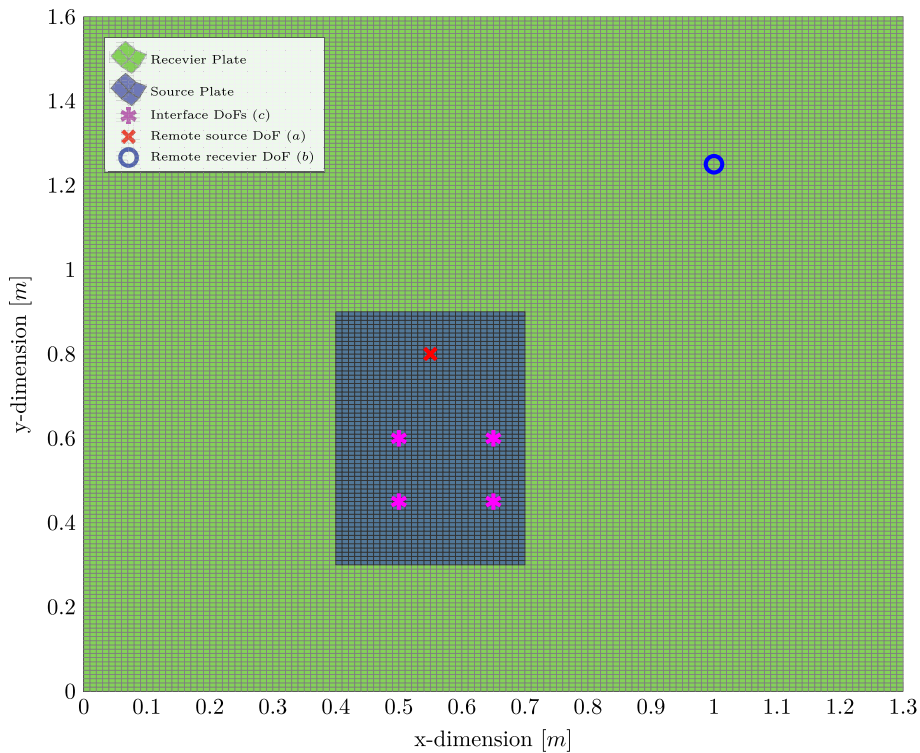


Fig. 9. Diagrammatic representation of the Finite Element (FE) numerical study. Two plates are coupled at 4 points (magenta stars) in the translational z and x/y rotational DoFs, α and β . Remote source (red cross) and receiver (blue cross) DoFs are also included. (For interpretation of the references to colour in this figure legend, the reader is referred to the web version of this article.)

Table 2

Geometry of the FE source and receiver plates. The material properties of each plate are; Young's modulus $E = 200 \times 10^9$ [N/m²], density $\rho = 8000$ [kg/m³], Poisson's ratio $\mu = 0.3$, with loss factors $\eta_s = 0.005$ and $\eta_R = 0.1$.

Plate	Dimensions ($x \times y \times z$) [m]
Source	$0.3 \times 0.6 \times 0.015$
Receiver	$1.3 \times 1.6 \times 0.01$

the MCC in Fig. 11c. From the assembly response prediction in Fig. 11d it is clear that MCC correctly identifies the artefacts arising due to inconsistencies between the blocked force and free mobility.

Comparing Figs. 10a and 11d it is further observed that the artefacts introduced in the operational response prediction, as indicated by the MCC, coincide with the blocked modes of the source sub-structure, i.e. the resonances in Fig. 10a. This is in agreement with the analytical example of inconsistency presented in Section 5.1.

As a final note regarding the numerical study presented above, the two inconsistencies can be seen to yield artefacts of a very different nature. The neglect of rotational DoFs, as in Section 5.4.1, leads to an erroneous prediction over a wide frequency range, whilst the inconsistency due to a perturbed natural frequency, as in Section 5.4.2, leads to localised artefacts. This appears to be in agreement with experimental observations [9].

6. Experimental case study

In this section the notion of completeness and consistency, as introduced above, along with their respective criteria, will be demonstrated as part of an experimental case study. The case study will be composed of two parts. In part 1 we will consider the characterisation of a blocked force and the completeness of the interface description used. In part 2 we will consider the consistency between the acquired blocked force and an experimentally obtained free source mobility.

The test structure is shown in Fig. 12; both rigid and resiliently coupled assemblies are considered. The source was a 3 footed aluminium plate with a servo-motor bolted to its centre (see Fig. 12d). The receiver structure was a steel beam framework. All resilient elements are considered part of the receiver. The source feet (i.e. the source-receiver interface) have been designed to facilitate characterisation in all 6 DoFs (see Fig. 12c). Each source foot was instrumented with 7 uni-axial

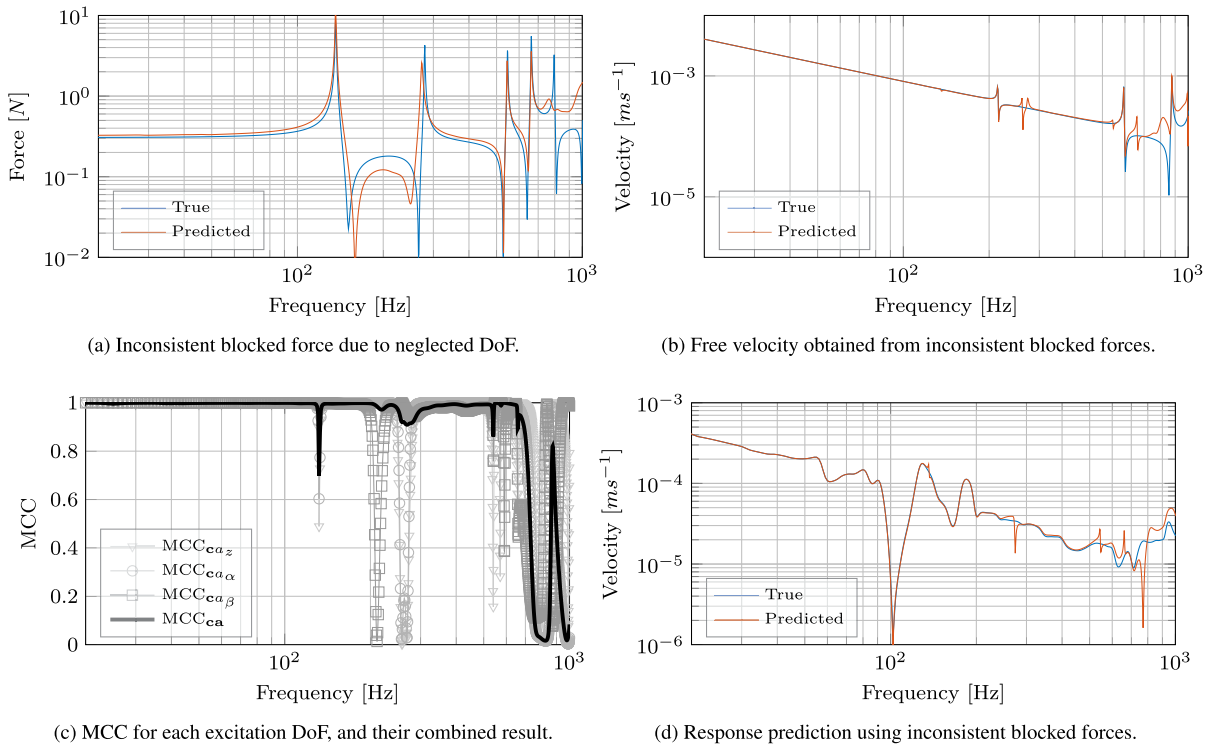


Fig. 10. Numerical results of the coupled FE plate model based on inconsistent blocked forces due to an incomplete interface description.

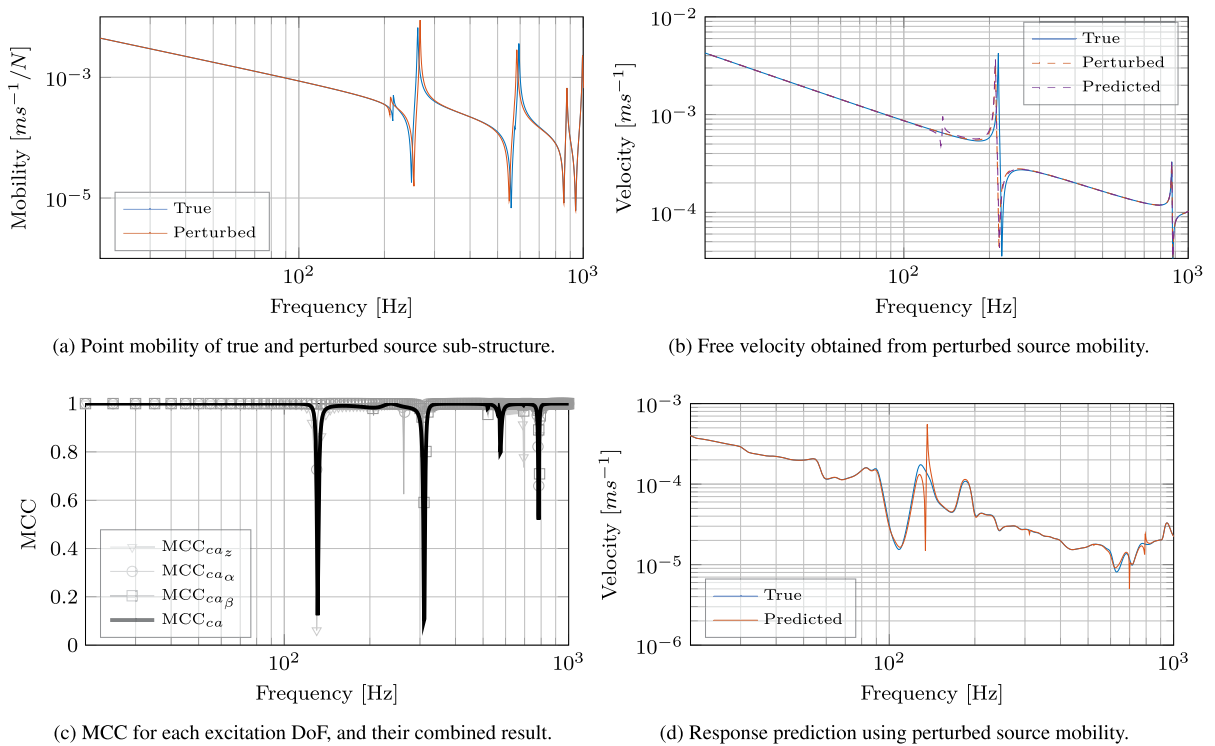


Fig. 11. Numerical results of the coupled FE plate model based on an inconsistent free source mobility.

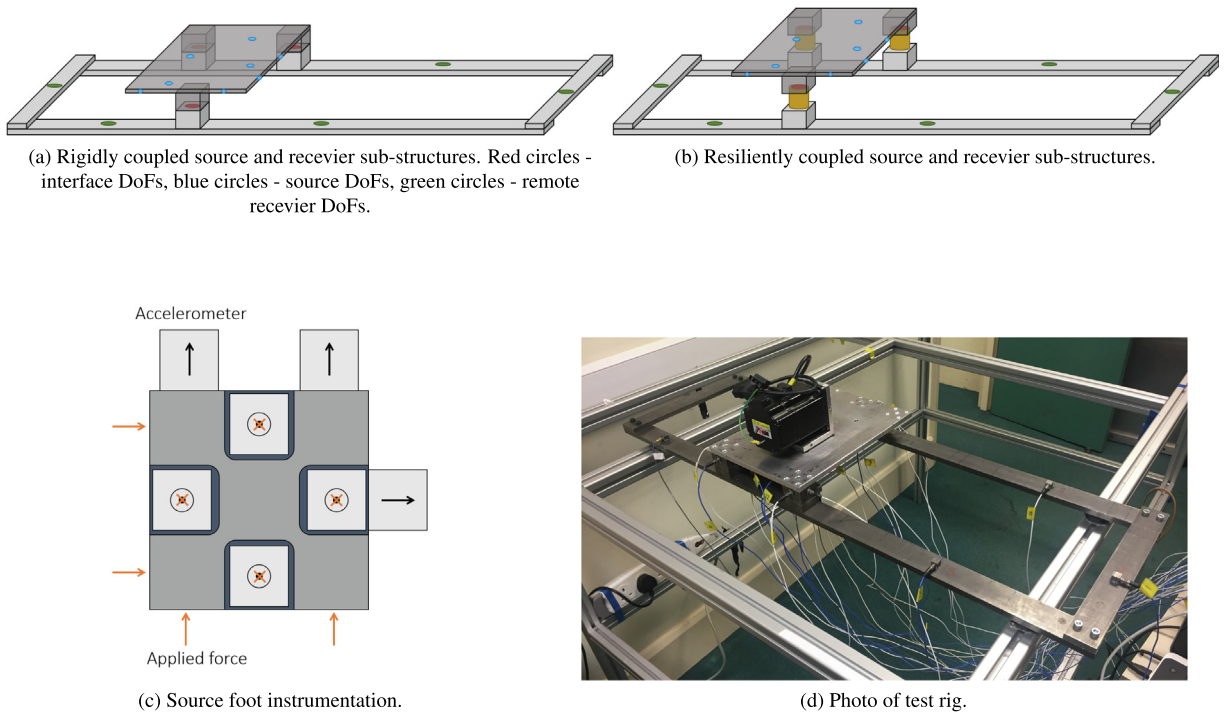


Fig. 12. Diagrammatic representations of experimental case study.

accelerometers as illustrated in Fig. 12c. Rotational DoFs were accounted for implicitly using an equivalent multi-point connection (EMPC) [30]. This approach was chosen over an explicit calculation of rotational components, for example using a finite difference approximation [31] or the virtual point transformation [32], due to its straight forward implementation and routine employment in practice.

Note that in what follows accelerance FRFs (\mathbf{A}) and accelerations (\mathbf{a}) have been used in place of mobility FRFs (\mathbf{Y}) and velocities (\mathbf{v}); all subscripts retain their previous meanings.

6.1. Completeness

In this section we will characterise the blocked force of the vibration source whilst under an operational condition (running at a constant 5000 rpm). This blocked force will then be used to predict the operational response at some remote receiver DoF (much like a standard in situ TPA procedure). This process will be repeated for 3 different interface descriptions.

To compute the ICC the following FRF matrices are measured, \mathbf{A}_{Ccc} , \mathbf{A}_{Cbc} , \mathbf{A}_{Cca} and \mathbf{A}_{Cba} . Of these, only the interface FRF matrix \mathbf{A}_{Ccc} is required by a standard blocked force characterisation. The remaining transfer FRFs constitute the additional measurements required to compute the ICC. The FRF \mathbf{A}_{Cbc} can be measured simultaneously to \mathbf{A}_{Ccc} with minimal effort other than including additional response sensors at some remote receiver DoFs b . The FRFs \mathbf{A}_{Cca} and \mathbf{A}_{Cba} require excitations to be made at some source side DoFs a , whilst simultaneously measuring the response at the interface and remote receiver DoFs, respectively. Note that these excitations need not coincide with any internal source DoFs, and can be chosen for convenience (so long as they sufficiently excite the interface modes). Provided the source is reasonably accessible, this would normally be practical and requires little additional effort. The ICC is then calculated as per Eq. (25).

In practice it is recommended that a) the ICC be computed prior to any operational measurements in case a more complete interface description is required, and b) that the source side excitations be applied in multiple directions to ensure that all interface modes are sufficiently excited. In this case study the (combined) ICC is computed for both rigid and resiliently coupled source-receiver assemblies (see Fig. 12). In each case 8 source side excitations (a , 4 in z , 2 in x and 2 in y) and 5 remote receiver DoFs (b , all in z) were considered. The measured FRFs were of the following dimensions: $\mathbf{A}_{\text{Ccc}} \in \mathbb{C}^{21 \times 21}$, $\mathbf{A}_{\text{Cbc}} \in \mathbb{C}^{5 \times 21}$, $\mathbf{A}_{\text{Cca}} \in \mathbb{C}^{21 \times 8}$ and $\mathbf{A}_{\text{Cba}} \in \mathbb{C}^{5 \times 8}$.

Shown in Fig. 13 are the translational x , y and z point FRFs at each foot of the source for both rigid (left) and resiliently (right) coupled assemblies. The highly resonant nature of the assembly considered clearly presents a more challenging experimental task than one that is well damped. For this reason the study considered may be deemed representative of the more challenging scenarios encountered in practice.

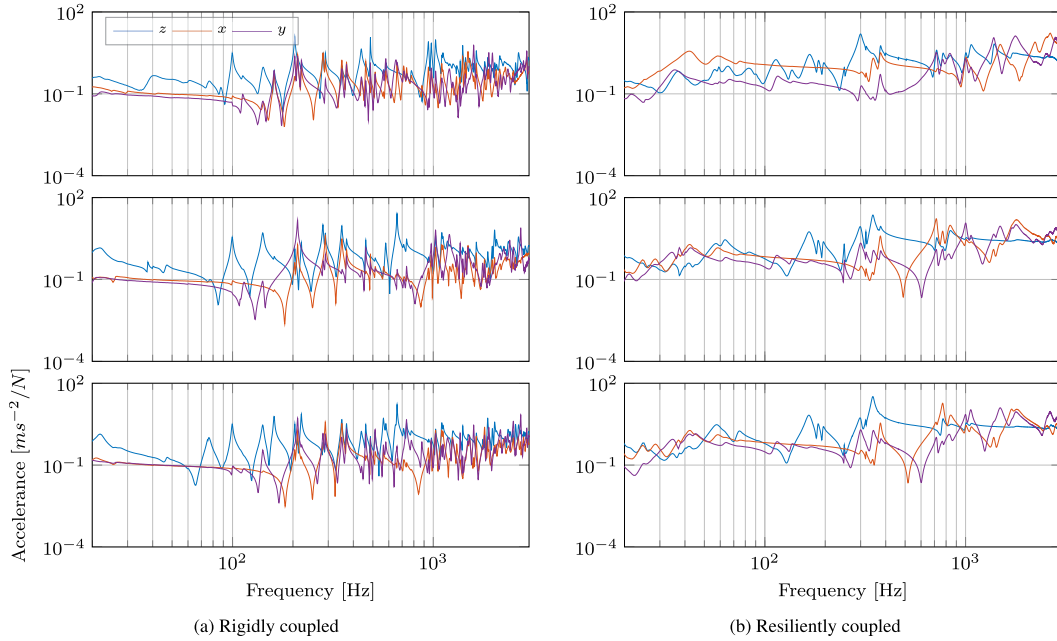


Fig. 13. Point accelerance of the rigidly (left) and resiliently (right) coupled source at each foot (top to bottom) in the translational z, x and y DoFs.

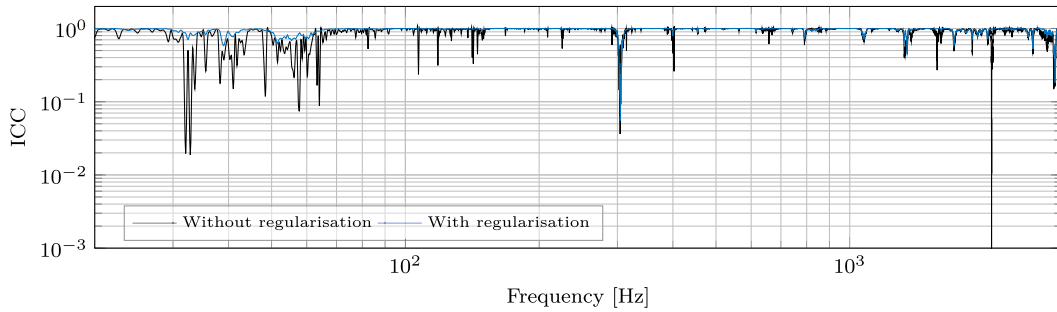
6.1.1. Rigid coupling

We will consider first the rigidly coupled assembly (see Fig. 12a). Note that hereafter only the combined ICCs will be presented, and that all results will be presented on a log y-scale for clarity. Shown in Fig. 14a in black is the ICC obtained when all interface DoFs (of which there were 21) are included. Assuming each foot behaves as a rigid contact (i.e. is described by 6 DoFs, 3 translational and 3 rotational), the interface description has redundancy; 21 interface DoFs have been included (7 per foot), yet only 18 are physically present. As such, it is proposed that the 3 smallest singular values may be discarded from the interface FRF matrix \mathbf{A}_{ccc} when its inversion is performed. This regularisation is applied to both the ICC calculation and any related blocked force predictions. The regularised ICC is shown in Fig. 14a in blue. A clear improvement is obtained over the un-regularised ICC. A similar result was observed when inspecting the corresponding blocked forces directly. This result demonstrates that the ICC is able to indicate an incompleteness not only due to physically absent DoFs, but an apparent incompleteness due to numerical and/or experimental error.

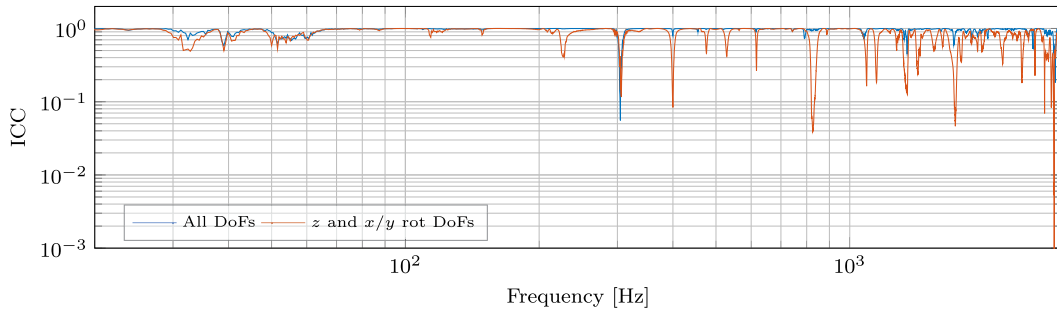
Shown in Fig. 14b and c are comparisons of the regularised ICC (including all DoFs) against the ICCs obtained using: translational z DoFs with x/y rotations (in orange) and translational z DoFs only (in purple). To obtain the z only DoFs the 4 translational z DoFs at each foot were averaged to obtain a pure vertical translation ($\mathbf{A}_{\text{ccc}} \in \mathbb{C}^{3 \times 3}$). The rotational x/y DoFs were implicitly included by retaining all 4 translational z DoFs at each foot ($\mathbf{A}_{\text{ccc}} \in \mathbb{C}^{12 \times 12}$), whilst discarding 3 singular values to remove redundancy. The ICC results of Fig. 14c indicate that the neglect of any DoFs worsens the interface description. For the rigidly coupled source considered here it appears that the rotational x/y DoFs are essential, and that the in-plane and rotational z (i.e. rotation around the z axis) DoFs can provide a noticeable improvement, particularly at high frequencies.

It is interesting to note that even when all DoFs are considered, there exists a notable incompleteness at approx. 300 Hz. Looking forward to Fig. 19a, it can be seen that this coincides with an artefact in the blocked force. Artefacts of this nature are common when dealing with highly resonant structures, such as the rigid assembly considered here, and can occur due to slight inconsistencies between measured FRFs [33].

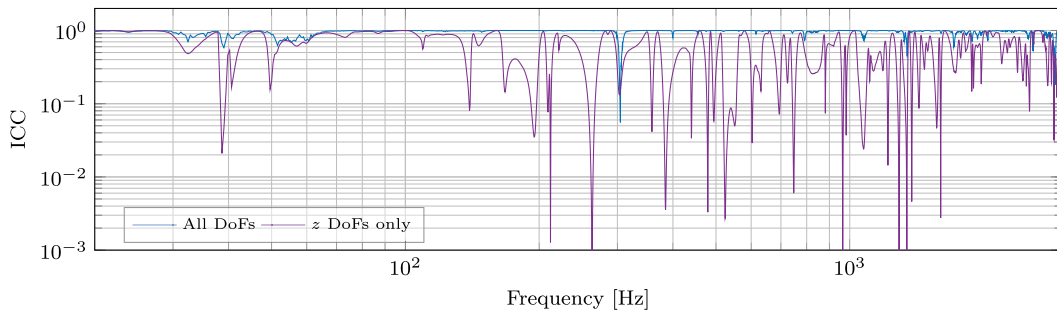
Based on the three interface descriptions whose ICCs are shown in Fig. 14, an operational response prediction is made using the acquired blocked force. Each prediction is compared against a directly measured response in Fig. 15. The left hand plots in Fig. 15 are shown in narrow band. The right hand plots are presented in 3rd octave bands for clarity. From top to bottom, each plot correspond to a prediction made with; all DoFs, z translations with x/y rotations, and z translations only. These results clearly mirror those of Fig. 14. The best response prediction is obtained when using all DoFs (i.e. a complete interface). A reasonable prediction is obtained when the contributions of in-plane and rotational z DoFs are neglected, particularly below approx 800 Hz. The prediction obtained when using only the translational z DoFs is poor, repeatedly over and under estimating the measured response, by over 5 dB in some regions. These results suggest that the ICC may be interpreted as a measure of quality in a blocked force characterisation, and used to indicate regions over which a poor prediction may be expected.



(a) Comparison of ICC with and without regularisation, calculated for all DoFs.



(b) Comparison of ICC obtained for different interface descriptions



(c) Comparison of ICC obtained for different interface descriptions

Fig. 14. ICC results obtained from the rigidly coupled assembly.

Note that for all predictions an over estimation is made at low frequencies below approx. 80 Hz. This is likely due to the poor coherence obtained, as a result of background noise, in some of the cross-FRF measurements. This effect is also seen in the ICC results of Fig. 14.

6.1.2. Resilient coupling

Based on the same interface descriptions as used above, we will now consider the resiliently coupled assembly. Shown in Fig. 16a is a comparison of the ICCs obtained for each of these interface descriptions. Fig. 16b compares the ICCs obtained from the rigid (blue) and resilient (orange) assemblies for the 'complete' interface description (i.e. all DoFs, with regularisation). Similarly, Fig. 16c compares the rigid (blue) and resilient (purple) ICCs obtained using the translational z DoFs only.

From Fig. 16a it that appears that at low frequencies, at least below 1 kHz, a reasonable interface description is obtained (indicated by an $ICC \approx 1$) using only the translational z DoFs. This is in stark contrast to the rigidly coupled case, as illustrated in Fig. 16c, where rotational DoFs were found to be essential. This result supports the argument that at low frequencies rotational DoFs can often be neglected for resiliently coupled structures. This is, however, not a general result, and there will undoubtedly exist resilient scenarios where rotational DoFs are essential. The role of rotational DoFs is more evident at high frequencies where, as shown in Fig. 16a, their inclusion noticeably improves the interface description (indicated by the ICC tending towards 1). It is interesting to note that by including the in-plane and rotational z DoFs little difference is made to the interface completeness.

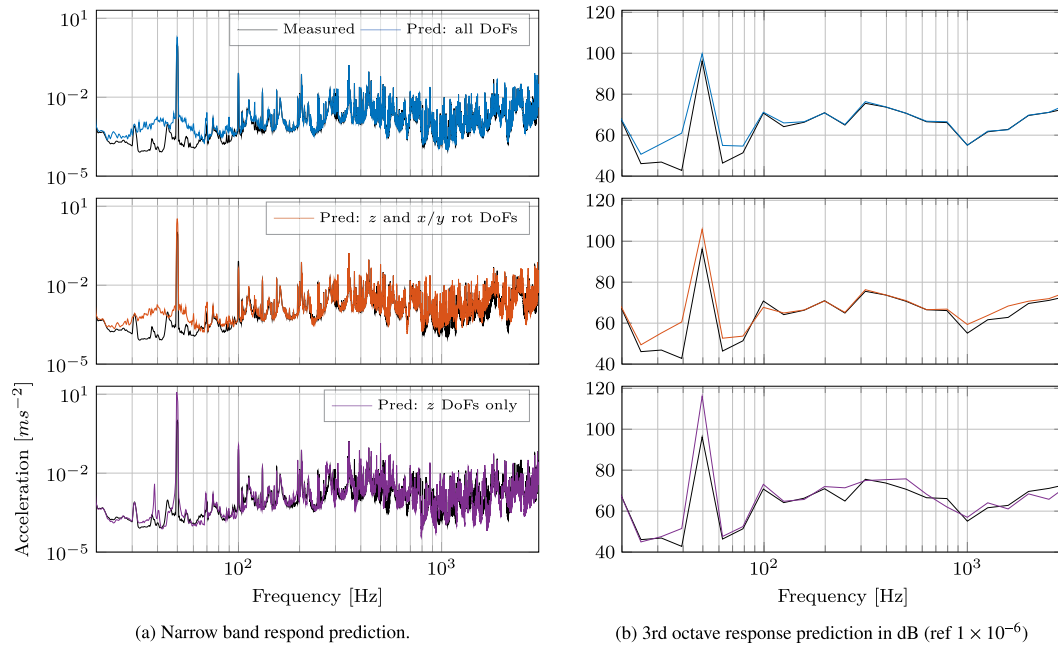


Fig. 15. Operational response prediction in the rigidly coupled assembly based on different interface descriptions. Black - directly measured response, blue - prediction using all DoFs, orange - prediction using vertical translations z and x/y rotations, purple - prediction using only vertical translations z . (For interpretation of the references to colour in this figure legend, the reader is referred to the web version of this article.)

As in the rigid case we observe the effect of measurement noise at low frequencies as causing an apparent incompleteness. For the resilient case a similar issue also arises at high frequencies, where signal attenuation through the resilient elements introduces noise, and therefore an apparent incompleteness.

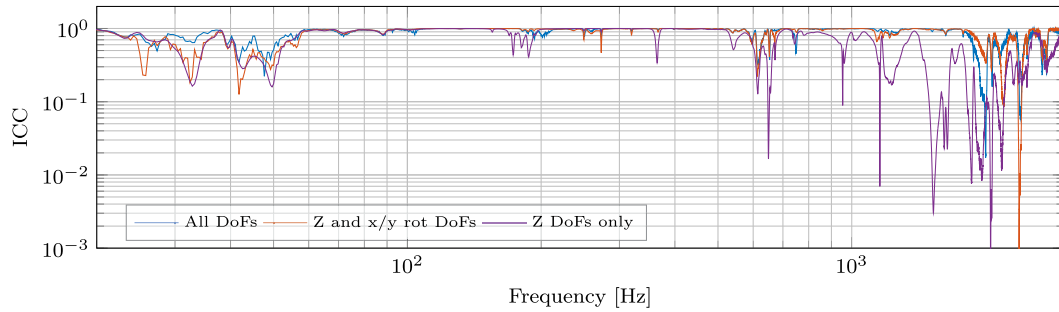
Shown in Fig. 17 are the operational response predictions made on the resiliently coupled assembly for the 3 interface descriptions considered above. Again, results are shown in narrow band (on the left) and 3rd octaves (on the right). From top to bottom, each plot corresponds to a prediction made with; all DoFs, z translations with x/y rotations, and z translations only. As expected, the accuracy of the predicted responses follow the trend of the ICCs presented in Fig. 16a. For the z only DoFs the response prediction is in good agreement up to approx. 1 kHz, beyond which we tend to under predict the measured response. This result is foreshadowed by the translational z only ICC in Fig. 16a. As indicated by the ICC, including the rotational x/y DoFs greatly improves the predicted response at high frequencies. Note that by further including the in-plane and rotational z DoFs worse agreement is obtained at high frequencies. This is likely because they do not contribute to the measured response, and so their inclusion introduces only noise and further experimental error. This is in contrast to the rigid case (see Fig. 15), where in-plane and rotational z DoFs were necessary to improve agreement at high frequencies. As in the rigid case we observe an over prediction at low frequencies. Again, this is likely due to noise encountered during the measurement of the FRFs.

The results presented through Figs. 14–17 demonstrate an application of the ICC when obtaining the blocked force for use in an operational response prediction on the same assembly (i.e. an in situ TPA application). The ICC may similarly be used when transferring the blocked force from one assembly (e.g. a test bench) to another (e.g. a Digital Twin), indicating regions where poor accuracy may be expected. An experimental example of this application, however, is considered beyond the scope of the present paper.

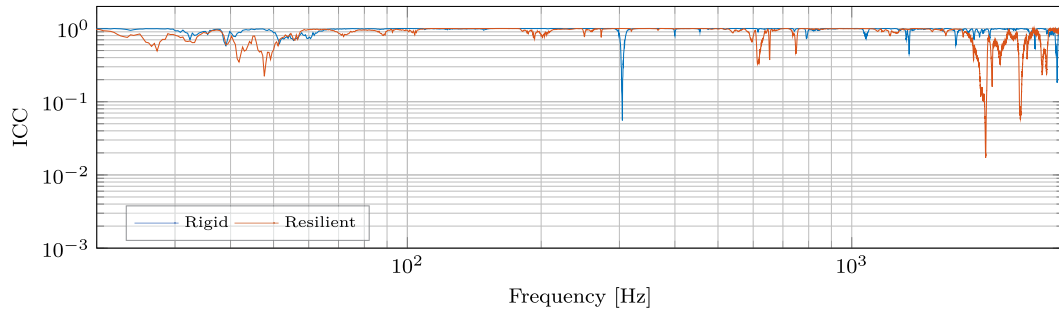
6.2. Consistency

In this section we will illustrate the notion of inconsistency using the experimental case study described above. In Section 5.3 a Measurement Consistency Criterion (MCC) was proposed to indicate at which frequencies inconsistencies were present. The MCC is a measure of similarity between a directly measured free velocity (due to a set of artificial excitations) and the free velocity calculated indirectly using an in situ blocked force (due to the same artificial excitation) and the free source mobility.

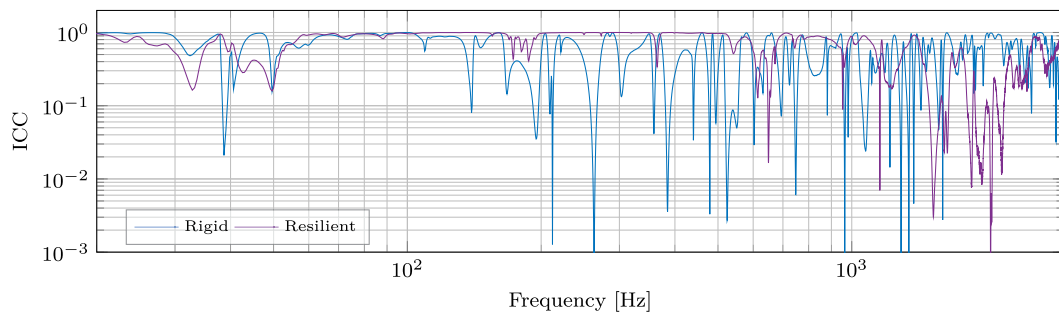
The issue of incompleteness is well defined, its cause being the neglect of interface DoFs. Inconsistency, however, can arise for a multitude of reasons (including incompleteness), many of which are difficult to replicate in a controlled manner on a simple laboratory structure. In what follows we will use the MCC to assess the consistency between the free source mobility and each blocked force obtained in Section 6.1 (i.e. for different levels of completeness).



(a) Comparison of resilient ICC obtained for different interface descriptions.



(b) Comparison of the rigid and resilient ICCs, calculated for all DoFs.



(c) Comparison of the rigid and resilient ICCs, calculated for translational z DoFs only. (Rigid result as in figure 14c)

Fig. 16. ICC results obtained from the resiliently coupled assembly.

Shown in Fig. 18 are the translational z point FRFs at each foot of the free source (remaining DoFs are omitted for clarity). Shown in Fig. 19a and b are the blocked forces obtained from the rigidly coupled assembly at one foot in the translational z direction, calculated using: all DoFs, translational z DoFs with x/y rotations, and translational z DoFs only. Shown in Fig. 19b are the equivalent set of blocked forces obtained from the resiliently coupled assembly. From Fig. 19a and b it is clear that the blocked forces obtained when using only the translational z DoFs are corrupted by artefacts. These artefacts are remnants of the coupled assembly that, due to the incomplete interface description, were not sufficiently 'removed' when characterising the blocked force. The blocked forces obtained when using all DoFs, and the translational z DoFs with x/y rotations, appear in good agreement with one another across the two assemblies. This demonstrates the independent nature of the blocked force, when obtained using a sufficiently complete interface description.

Shown in Fig. 20a and b are the free response predictions (due to an artificial excitation), at one foot of the source in the translational z DoF, based on the blocked forces shown in Fig. 19a and b, respectively. Also shown, in black, is the directly measured free response. According to Section 5, the discrepancies observed between directly measured and predicted free responses are due to inconsistencies between the free acceleration and the acquired blocked force.

In the rigid case we obtain a reasonable free response prediction when all DoFs are included. When only the translational z DoFs are considered, a poor prediction is obtained with numerous artefacts present. These artefacts can be seen to coincide with many of those in the corresponding blocked force (i.e. the purple plot in Fig. 19a). This result may be interpreted as so. The blocked force acquired when using an incomplete interface description will be the true blocked force plus a contribution from the unknown DoFs,

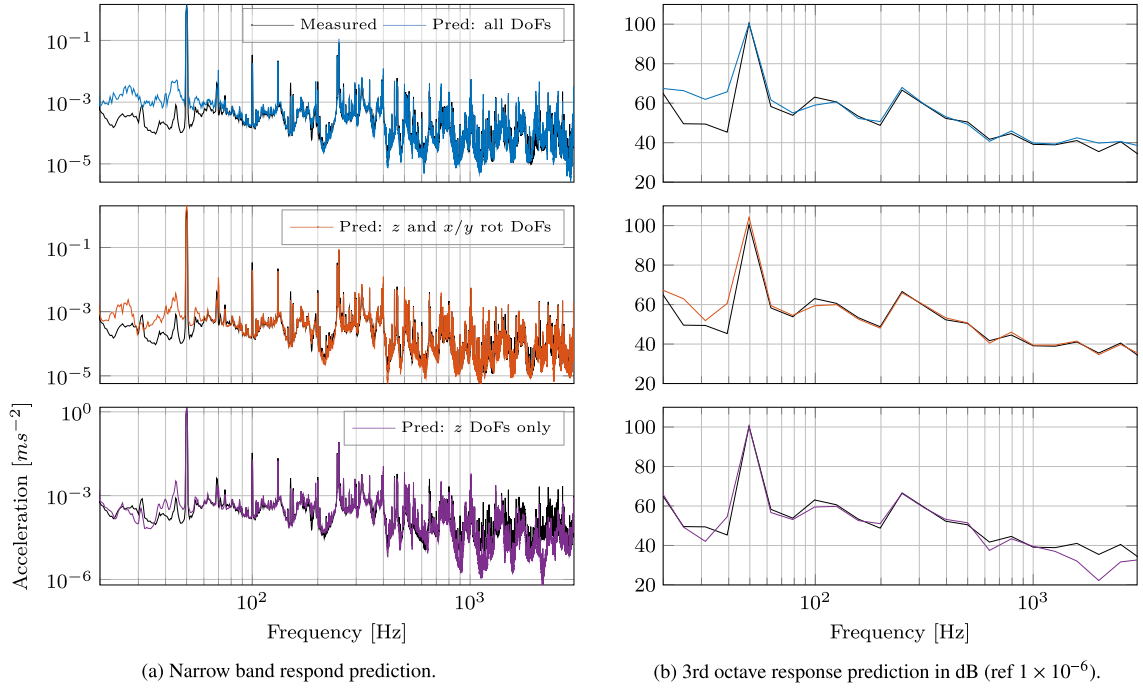


Fig. 17. Operational response prediction in the resiliently coupled assembly based on different interface descriptions. Black – directly measured response, blue – prediction using all DoFs, orange – prediction using vertical translations z and x/y rotations, purple – prediction using only vertical translations z . (For interpretation of the references to colour in this figure legend, the reader is referred to the web version of this article.)

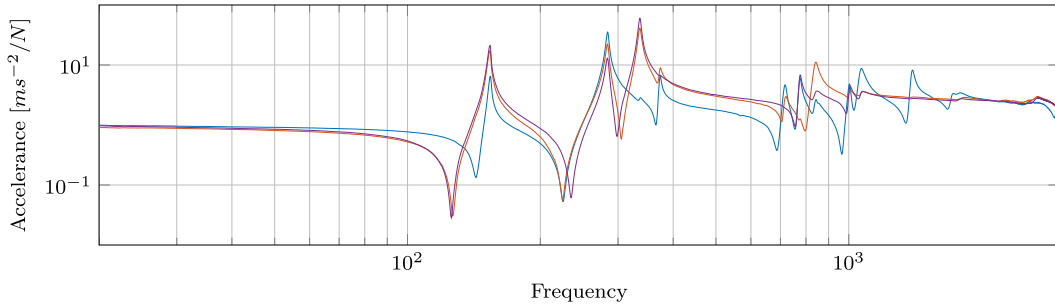


Fig. 18. Free source acceleration at each foot in the translational z DoF.

$$\ddot{\mathbf{f}}_{\text{C}c_j} = \bar{\mathbf{f}}_{\text{S}c_j} + \mathbf{A}_{\text{C}c_j c_j}^{-1} \mathbf{A}_{\text{C}c_j c_j} \bar{\mathbf{f}}_{\text{S}c_j} \tag{47}$$

where Eq. (7) has been rewritten in terms of acceleration. To predict the free source response we use the free source acceleration as so,

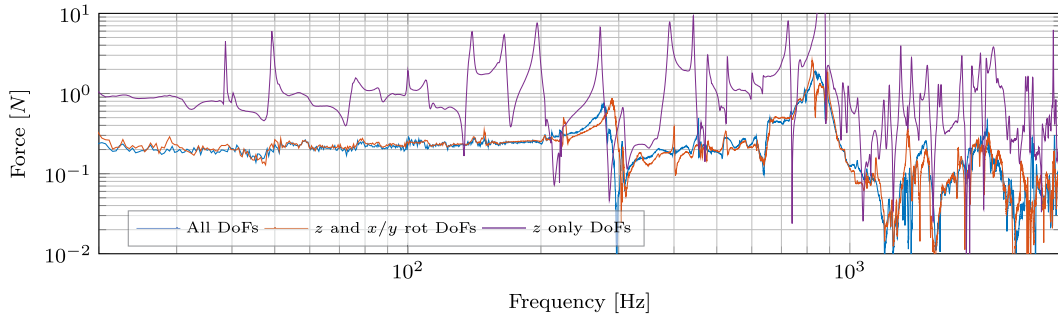
$$\mathbf{a}_{\text{S}c_j} = \mathbf{A}_{\text{S}c_j c_j} \ddot{\mathbf{f}}_{\text{C}c_j}. \tag{48}$$

Substituting the acquired blocked force leads to,

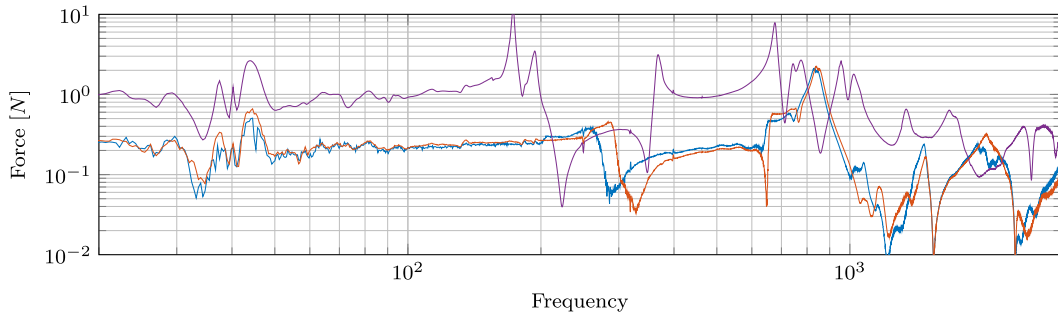
$$\ddot{\mathbf{a}}_{\text{S}c_j} = \mathbf{A}_{\text{S}c_j c_j} \bar{\mathbf{f}}_{\text{S}c_j} + \mathbf{A}_{\text{S}c_j c_j} \mathbf{A}_{\text{C}c_j c_j}^{-1} \mathbf{A}_{\text{C}c_j c_j} \bar{\mathbf{f}}_{\text{S}c_j}. \tag{49}$$

For the true free response to be obtained, the blocked force $\bar{\mathbf{f}}_{\text{S}c_j}$ must contribute through the FRF $\mathbf{A}_{\text{S}c_j c_j}$. This would require $\mathbf{A}_{\text{S}c_j c_j} \mathbf{A}_{\text{C}c_j c_j}^{-1} \mathbf{A}_{\text{C}c_j c_j} \stackrel{?}{=} \mathbf{A}_{\text{S}c_j c_j}$. Clearly, for the rigidly coupled source this is not the case, and so the neglected blocked force $\bar{\mathbf{f}}_{\text{S}c_j}$ manifest itself as an artefact in the free response. By including the rotational x/y DoFs, the effective contribution of $\bar{\mathbf{f}}_{\text{S}c_j}$ is reduced, and so a more accurate free response prediction is obtained, as in Fig. 20a.

For the resilient case a reasonable free response prediction is obtained irrespective of the interface description. This result may be interpreted as so. The free and resiliently coupled source accelerances are approximately equal to one another in the

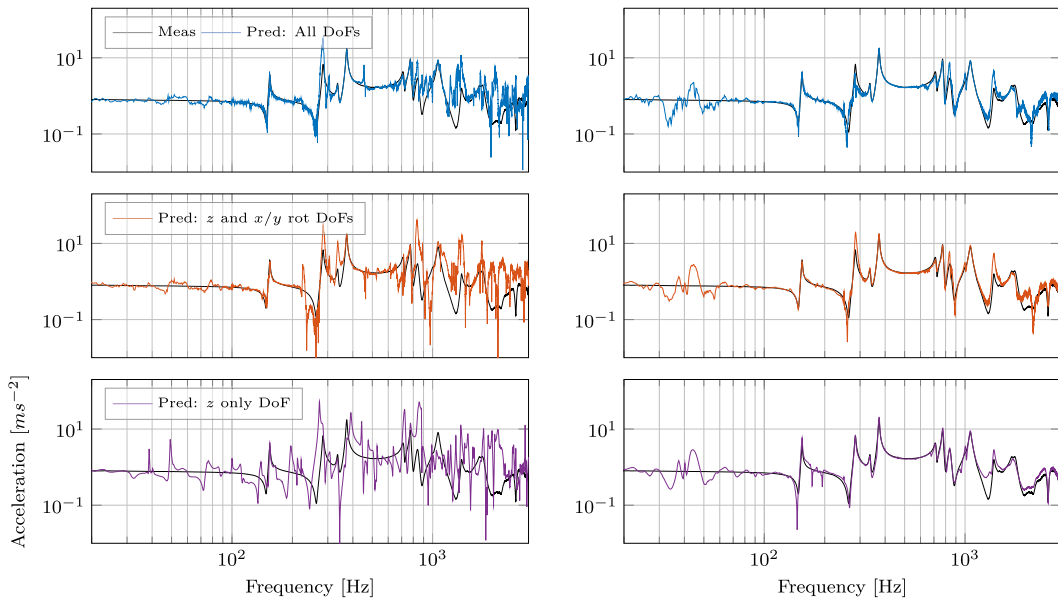


(a) Rigidly coupled source.



(b) Resiliently coupled source.

Fig. 19. Translational z blocked force obtained from rigid (top) and resiliently (bottom) coupled assemblies using: all DoFs (blue), translational z with x/y rotations (orange), and translational z DoFs only (purple). (For interpretation of the references to colour in this figure legend, the reader is referred to the web version of this article.)



(a) Rigidly coupled source.

(b) Resiliently coupled source.

Fig. 20. Translational z free acceleration prediction based on the blocked forces obtained from rigid (a) and resilient (b) assemblies using: all DoFs (blue), translational z with x/y rotations (orange), and translational z DoFs only (purple). The directly measured free response is shown in black. (For interpretation of the references to colour in this figure legend, the reader is referred to the web version of this article.)

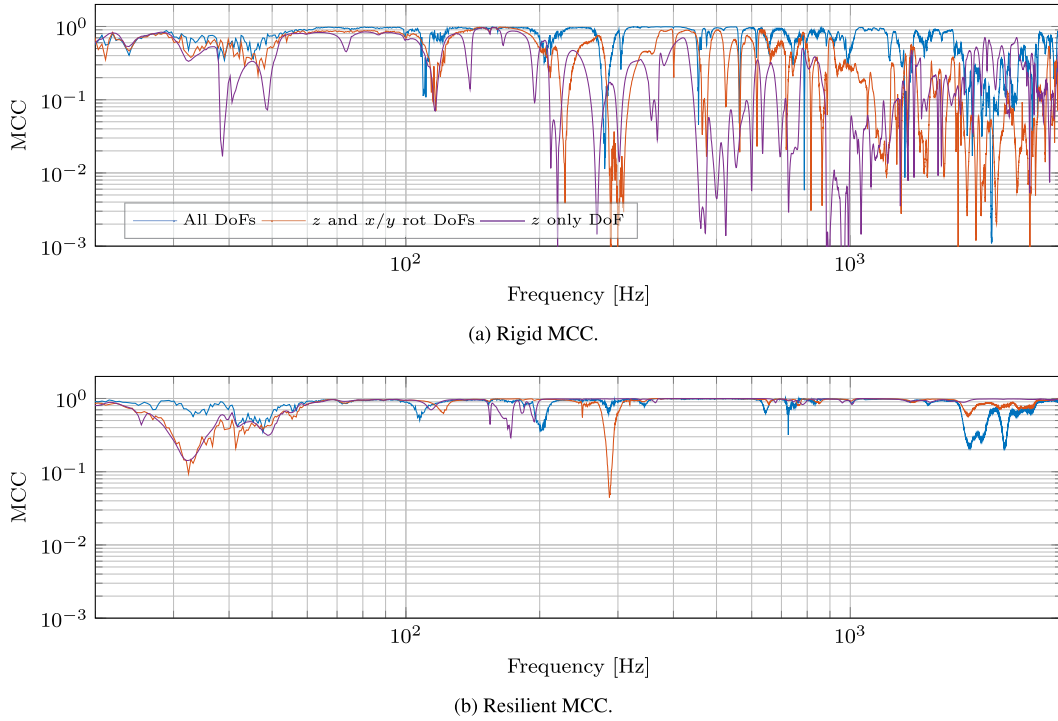


Fig. 21. MCC results obtained from the rigid and resiliently coupled assembly.

mid to high frequency range. As such, we have that $\mathbf{A}_{\mathbf{s}_c \mathbf{c}_c} \mathbf{A}_{\mathbf{c}_c \mathbf{c}_c}^{-1} \approx \mathbf{I}$, and that $\mathbf{A}_{\mathbf{c}_c \mathbf{c}_c} \approx \mathbf{A}_{\mathbf{s}_c \mathbf{c}_c}$. Consequently, even though the unknown DoFs were neglected in the blocked force characterisation, their contribution $\mathbf{f}_{\mathbf{s}_c}$ is propagated correctly onto the free response prediction. This is due to the dynamic similarity of the characterisation assembly (resilient) and prediction assembly (free).

The results of Fig. 20 are somewhat intuitive. They demonstrate that it is easier to predict the free response of a source when using a blocked force obtained from a resilient assembly. On a rigid assembly the source is physically constrained in all DoFs, and so to ‘remove’ the effect of these constraints *all* DoFs must be included in its characterisation. On a resilient assembly the source is far less constrained and so fewer DoFs are required to predict an accurate free response.

Like the free response prediction considered above, to successfully predict the operational response in an *assembled* structure we require a cancellation of the same FRF terms between the blocked force and the coupled assembly FRF (see Eq. (41)). As such, we might expect artefacts similar to those observed in Fig. 20a to appear in an operational response prediction. Whilst Fig. 20 illustrates the issue of inconsistency, it does so using a single interface DoF. The MCC provides a measure of consistency across the entire set of interface DoFs. Shown in Fig. 21 are the MCCs corresponding to each of the free response predictions shown in Fig. 20.

The MCCs clearly mirror the conclusions made above. For the rigidly coupled case, poor consistency is obtained unless all DoFs are included. That is to say, to predict the free response from a rigidly coupled blocked force, all DoFs must be accounted for. This poor consistency indicates a more likely presence of artefacts in a response prediction. For the resilient case, we see again that a good level of consistency is achieved irrespective of how many DoFs are included.

7. Conclusion

The primary aim of this paper has been to introduce the notions of completeness and consistency with regards to the characterisation and application of an in situ blocked force. It is noted, however, that these concepts apply more generally to both sub-structure coupling and de-coupling also.

The in situ blocked force method has become the most promising approach for the independent characterisation of vibratory sources, yet few works have considered the potential sources of systematic errors. In the present paper we have identified the notions of completeness and consistency as two likely sources.

Completeness is related to the interface description adopted when characterising the blocked force (i.e the number/orientation of DoFs at the interface). It has been shown both numerically and experimentally that an incomplete interface description can lead to the introduction of systematic errors in a blocked force characterisation. To this end, an Interface Completeness Criterion (ICC) has been proposed to quantify the degree of completeness that an interface possesses. The

ICC is calculated using coupled assembly FRFs and is therefore available from in situ measurements. It may be interpreted as a level of confidence in the acquired blocked force, and could thus serve as an appropriate measure of model uncertainty when blocked forces are transferred between OEMs and manufactures. The ICC may find further use in the assessment of interface descriptions for sub-structure decoupling procedures.

The notion of consistency relates to the underlying dynamics shared by active and passive quantities in an operational assembly. Sources of inconsistency are less well defined, and can arise for a multitude of reasons, such as: incompleteness, a change in the passive properties of a vibration source during the active and passive phases of a blocked force characterisation, a change in the source properties between installed and free states, errors when modelling numerically the passive properties of a source, among others. It has been shown that inconsistencies between the blocked force and an assembly's FRF matrix can introduce artefacts in a response prediction. A criterion has been proposed to identify inconsistencies between an acquired blocked force and the free FRF matrix of a vibration source. The Measurement Consistency Criterion (MCC) has been demonstrated using numerical and experimental examples and shown to correctly indicate the frequencies over which inconsistencies are present. The issue of consistency is of particular relevance if, for example, an experimental blocked force is to be combined with a numerical source model. In this case consistency is unlikely to be achieved without some additional modelling effort.

The general application of in situ blocked forces as a means of modelling the complex mechanisms that lead to vibratory excitation has broad applications across a variety of industries. Nevertheless, an understanding of the uncertainties involved is essential, and worthy of future research effort.

CRediT authorship contribution statement

J.W.R. Meggitt: Conceptualization, Methodology, Validation, Investigation, Writing - original draft, Writing - review & editing. **A.T. Moorhouse:** Conceptualization, Writing - review & editing, Supervision, Funding acquisition.

Declaration of Competing Interest

The authors declare that they have no known competing financial interests or personal relationships that could have appeared to influence the work reported in this paper.

Acknowledgements

This work was part funded through the EPSRC Research Grant EP/P005489/1 Design by Science. The authors would like to acknowledge the valuable contributions of A. Clot and R.S Langley from the University of Cambridge.

References

- [1] A.T. Moorhouse, B.M. Gibbs, Measurement of structure-borne sound emission from resiliently mounted machines in situ, *J. Sound Vib.* 180 (1) (1995) 143–161, <https://doi.org/10.1006/jsvi.1995.0071>.
- [2] J.W. Verheij, Multi-path sound transfer from resiliently mounted shipboard machinery. PhD thesis, TNO, 1982.
- [3] A.S. Elliott, A.T. Moorhouse, T. Huntley, S. Tate, In-situ source path contribution analysis of structure borne road noise, *J. Sound Vib.* 332 (24) (2013) 6276–6295.
- [4] F.X. Magrans, Method of measuring transmission paths, *J. Sound Vib.* 74 (3) (1981) 321–330.
- [5] D. De Klerk, A. Ossipov, Operational transfer path analysis: theory, guidelines and tire noise application, *Mech. Syst. Signal Processing* 24 (7) (2010) 1950–1962.
- [6] M.V. van der Seijs, D.D. Klerk, D.J. Rixen. General framework for transfer path analysis: History, theory and classification of techniques. *Mechanical Systems and Signal Processing*, pages 1–28, 2015..
- [7] A.T. Moorhouse, Virtual acoustic prototypes: Listening to machines that don't exist, *Acoust. Australia* 33 (2005) 97–105.
- [8] J.W.R. Meggitt, A.S. Elliott, A.T. Moorhouse, Virtual assemblies and their use in the prediction of vibro-acoustic responses, in: *Proceedings of the Institute of Acoustics Warwickshire*, 2016.
- [9] A. Clot, J.W.R. Meggitt, R.S. Langley, A.S. Elliott, A.T. Moorhouse, Development of a hybrid FE-SEA-experimental model, *J. Sound Vib.* 452 (2019) 112–131.
- [10] F. Fahy, J. Walker, *Advance Applications in Acoustics, Noise and Vibration*, Spon Press, 2004.
- [11] A.T. Moorhouse, A.S. Elliott, T.A. Evans, In situ measurement of the blocked force of structure-borne sound sources, *J. Sound Vib.* 325 (4–5) (sep 2009) 679–685.
- [12] J.W.R. Meggitt, A.S. Elliott, A.T. Moorhouse, A covariance based framework for the propagation of uncertainty through inverse problems with an application to force identification, *Mech. Systems Signal Process.* 124 (2019) 275–297.
- [13] T. ten Wolde, G. Gadefelt, Development of Standard Measurement Methods for Structureborne Sound Emission, *Noise Control Eng. J* 28 (1) (1987) 5.
- [14] D. Zabel, M. Sturm, T. Alber, A.T. Moorhouse, Embedded MEMS accelerometers for the in-situ measurement of blocked forces in coupled structures, *DAGA 1* (2017) 7–10.
- [15] Y.I. Bobrovnikskii, A theorem on the representation of the field of forced vibrations of a composite elastic system, *Acoust. Phys.* 47 (5) (2001) 586–589.
- [16] D. Lennström, M. Olsson, F. Wullens, A. Nykänen, Validation of the blocked force method for various boundary conditions for automotive source characterization, *Appl. Acoust.* 102 (2016) 108–119.
- [17] K. Wiene, M. Sturm, A.T. Moorhouse, J.W.R. Meggitt, Robust NVH engineering using experimental methods – Source characterization techniques for component transfer path analysis and virtual acoustic prototyping, in: *SAE Noise and Vibration Conference & Exhibition, Detroit, USA, 2019*.
- [18] H.K. Lai, *Alternative test methods for measuring structure-borne sound power*, Internoise, Honolulu, Hawaii, USA, 2006.
- [19] G. Banwell, R. Faventi, Assessment of experimental techniques to characterise the vibration source strength of a motor radially mounted with resilient elements, ISMA, Leuven, 2016.
- [20] G. Banwell, Christopher Monk, Simultaneous air-borne and structure-borne characterisation of in-situ ducted sources, ICSV25, Hiroshima, Japan, 2018.

- [21] A.S. Elliott, A.T. Moorhouse, In-situ characterisation of structure borne noise from a building mounted wind turbine, *ISMA* (2010) 2055–2068.
- [22] D. Miguez, O. Farrell, K. Samami, R. Arbabi, A.T. Moorhouse, A.S. Elliott, Application of dynamic substructuring and in situ blocked force method for structure borne noise prediction in a reverberation, *Proc. Inst. Acoust.* 41 (2019) 255–263.
- [23] J.W.R. Meggitt, A.S. Elliott, A.T. Moorhouse, A. Clot, R.S. Langley, Development of a hybrid FE-SEA-experimental model: experimental subsystem characterisation, *NOVEM: Noise and Vibration - Emerging Methods*, Ibiza, 2018.
- [24] A. Clot, R.S. Langley, J.W.R. Meggitt, A.T. Moorhouse, A.S. Elliott, Development of a hybrid FE-SEA-experimental model: theoretical formulation, *NOVEM: Noise and Vibration - Emerging Methods*, Ibiza, 2018.
- [25] J.W.R. Meggitt, A.T. Moorhouse, A.S. Elliott, On the problem of describing the coupling interface between substructures: an experimental test for 'completeness', *Proceedings of the 36th International Modal Analysis Conference - IMAC*, vol. 4, 2018, pp. 1–12, Conference Proceedings of the Society for Experimental Mechanics Series.
- [26] A.T. Moorhouse, A.S. Elliott, The 'round trip' theory for reconstruction of Green's functions at passive locations, *J. Acoust. Soc. Am.* 134 (5) (Nov 2013) 3605–3612.
- [27] A. Elliott, A. Moorhouse, J.W.R. Meggitt, Identification of Coupled Degrees of Freedom at the Interface Between Sub-structures, in: *NOVEM: Noise and Vibration - Emerging Methods*, Ibiza, Spain, 2018, pp. 1–9.
- [28] J.W.R. Meggitt, On the treatment of uncertainty in experimentally measured frequency response functions, *Metrologia* 55 (2018) 806–818.
- [29] M. Petyt, *Introduction to Finite Element Vibration Analysis*, 2nd edition, Cambridge University Press, 2010.
- [30] D.D. Klerk, D.J. Rixen, S.N. Voormeeren, F. Pasteuning, Solving the RDoF Problem in Experimental Dynamic Substructuring, in: *Proceedings of the 26th International Modal Analysis Conference - IMAC*, 2008.
- [31] A.S. Elliott, A.T. Moorhouse, G. Pavić, Moment excitation and the measurement of moment mobilities, *J. Sound Vib.* 331 (1) (2012) 2499–2519.
- [32] M.V. van der Seijs, D. van den Bosch, D. de Klerk, An improved methodology for the virtual point transformation of measured frequency response functions in dynamic substructuring, *4th ECCOMAS Thematic Conference on Computational Methods in Structural Dynamics and Earthquake Engineering*, number 4, Kos Island, Greece, 2013.
- [33] D.J. Rixen, How measurement inaccuracies induce spurious peaks in frequency based substructuring, in: *Proceedings of the 26th International Modal Analysis Conference - IMAC*, Orlando, Florida, 2008.